nanomaterials

MDPI

Review

Interfacial Coupling and Modulation of van der Waals Heterostructures for Nanodevices

Kun Zhao, Dawei He, Shaohua Fu, Zhiying Bai, Qing Miao, Mohan Huang, Yongsheng Wang * and Xiaoxian Zhang *

Key Laboratory of Luminescence and Optical Information, Ministry of Education, Institute of Optoelectronic Technology, Beijing Jiaotong University, Beijing 100044, China
* Correspondence: yshwang@bjtu.edu.cn (Y.W.); zhxiaoxian@bjtu.edu.cn (X.Z.)

Abstract: In recent years, van der Waals heterostructures (vdWHs) of two-dimensional (2D) materials have attracted extensive research interest. By stacking various 2D materials together to form vdWHs, it is interesting to see that new and fascinating properties are formed beyond single 2D materials; thus, 2D heterostructures-based nanodevices, especially for potential optoelectronic applications, were successfully constructed in the past few decades. With the dramatically increased demand for well-controlled heterostructures for nanodevices with desired performance in recent years, various interfacial modulation methods have been carried out to regulate the interfacial coupling of such heterostructures. Here, the research progress in the study of interfacial coupling of vdWHs (investigated by Photoluminescence, Raman, and Pump–probe spectroscopies as well as other techniques), the modulation of interfacial coupling by applying various external fields (including electrical, optical, mechanical fields), as well as the related applications for future electrics and optoelectronics, have been briefly reviewed. By summarizing the recent progress, discussing the recent advances, and looking forward to future trends and existing challenges, this review is aimed at providing an overall picture of the importance of interfacial modulation in vdWHs for possible strategies to optimize the device's performance.

Keywords: van der Waals heterostructure; interfacial interaction; modulation; devices

Citation: Zhao, K.; He, D.; Fu, S.; Bai, Z.; Miao, Q.; Huang, M.; Wang, Y.; Zhang, X. Interfacial Coupling and Modulation of van der Waals Heterostructures for Nanodevices. *Nanomaterials* **2022**, *12*, 3418. https://doi.org/10.3390/nano12193418

Academic Editors: Yann-Wen Lan and Der-Hsien Lien

Received: 17 August 2022
Accepted: 23 September 2022
Published: 29 September 2022

1. Introduction

Along with the rise of graphene, alternative layered two-dimensional (2D) materials, which consist of strong in-plane covalent bonds and weak intra-plane van der Waals bonds, have attracted tremendous attention all around the world. The easy exfoliation into stable atomically thin materials, together with the dimensionality effect, induced fascinating properties, enabling the construction of various devices with smaller sizes and fewer defects [1]. Especially, 2D materials, such as transition metal dichalcogenides (TMDs), transition metal carbides or carbon-nitrides (Mxenes), and boron nitride (BN) [2–4], are extremely thin, transparent, and flexible, allowing for transparent devices to be made in flexible circuit materials [5–7]. TMDs have excellent properties, such as large surface area, great mechanical properties, high mobility, large exciton binding energy and long exciton lifetime, etc., thus providing unprecedented access to the exploration of new physics in such quantum systems, and meanwhile promote the applications of electronic and optoelectronic devices [8–10]. Currently, various devices with high performance have been developed based on 2D materials, such as field effect transistors (FETs) for logic circuits, radio-frequency devices, chemical sensing, optoelectronic devices, memristors, etc. [10–13]. The research progress of 2D materials, including the synthesis of 2D materials, the exploration of new physics, and the applications of various devices, has been comprehensively reviewed by many papers [10,14–18] and inspired a lot of researchers in related fields.

With the development of 2D materials, researchers have focused on the study of the van der Waals (vdW) heterostructure due to the increasing demand for excellent junctions in

the semiconductor industry. Different from traditional semiconductor heterojunctions, high-quality vdW heterostructures (vdWHs) can be fabricated by simply stacking two layers of 2D materials together, similar to Lego [16,19–22]. Note that, obviously, more layers of 2D materials can be stacked together to build more complicated vdWHs if necessary, but currently, most of the research work still focuses on the vdWHs consisting of two kinds of materials. Integrating different 2D materials to form various vdWHs can effectively broaden the variety of physical properties and create novel device structures without considering the lattice matching in highly different material systems. Furthermore, inspired by such 2D/2D TMD vdWHs, organic semiconductors with similar conjugated structures have been utilized to fabricate organic–inorganic vdWHs, which also holds great potential for building multifunctional flexible nanodevices with even higher performance for future electronics and optoelectronics. At present, various devices based on such 2D-structured vdWHs (including both inorganic 2D/2D vdWHs and organic–inorganic vdWHs), such as new types of solar cells and photodetectors [23–25], photoelectric memories [26–28] and other two-dimensional devices [29–32], have been reported.

However, the realization of such electronic and optoelectronic devices is dominated by the fundamental understanding of the interface. In order to achieve the predictable utilization of vdWHs in such devices, the understanding and control of the key parameters in the device metrics must be solved. Therefore, it is necessary to characterize the actual electronic structure of the heterostructure interfaces, such as interfacial dipole interaction, local charge transfer, and the resulting kinetic processes, such as the carrier relaxation paths and the decay times, and explore the methods that can effectively modulate these microscopic processes to optimize the physical properties and thus improve the device performance.

Herein, we review the latest research progress in the interfacial coupling of vdWHs, including inorganic 2D heterostructures and organic–inorganic heterostructures. First, research progress in the various methods to fully characterize the interfacial coupling of vdWHs was summarized, including (1) stable-state optical methods such as optical absorption, photoluminescence (PL), and Raman spectroscopies, (2) transient optical methods, such as pump–probe spectroscopy, transient absorption spectroscopy, and transient electronic sum frequency generation spectroscopy, etc., and (3) other techniques such as Kelvin probe force microscopy (KPFM), scanning tunneling microscopy (STM), piezoresponse force microscopy (PFM) et al. Moreover, we also review the recent modulation strategies of the interfacial coupling of vdWHs. The modulation part is divided into four parts: (1) strain engineering modulation, (2) electric field modulation, (3) optical field modulation, and (4) "twisted angle" modulation. In order to make this review paper easier to understand, we have drawn the main structure of this review in the schematic illustration shown in Figure 1. Generally, this paper only briefly summarizes the research progress related to vdWHs interfacial coupling, hoping to provide some basic information for researchers or students who are new to this field.

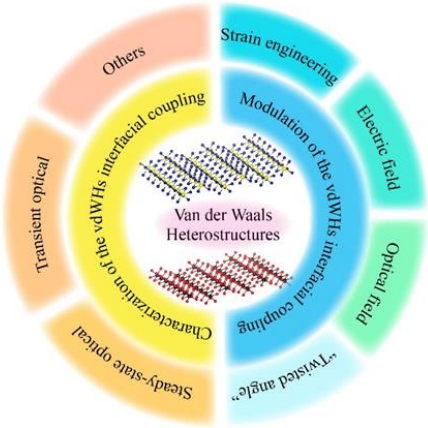

Figure 1. Schematic illustration of the main contents in this review.

2. Various Characterization Methods to Investigate the Interfacial Coupling of vdWHs

Heterostructures are widely utilized as a basic building block in advanced semiconductor devices, such as field effect transistors (FET), light-emitting diodes, and so on. Generally, there are three types of heterostructures, i.e., type I, type II, and type III (Figure 2). Type I arrangements can be used for energy transfer and are widely applied in organic light-emitting diodes (OLEDs) [33]. Whereas the type II arrangements enable efficient electron/hole separation at interfaces of optoelectronic devices, such as photodetectors [34], photodiodes [35], and photovoltaics [36]. Compared to the other two heterostructures, however, the type III arrangements are less common and rarely utilized in the semiconductor industry [37]. Since this review paper targets the potential applications of vdWHs for further electronics and optoelectronics, we will mainly focus on the type II arrangements here. Some of the identified types of vdWHs in the review are listed in Table 1. In order to apply vdWHs to practical electric and optoelectronic applications, it is essential to have a clear understanding of interfacial physics, such as interlayer coupling, charge transfer, exciton formation, and dynamics. By fully characterizing the electronic structure, optical response, and optoelectronic properties, including interfacial energy level alignment without and under illumination, charge transfer, light absorption, and emission, etc., we could obtain key information for device design and optimization in the future. Currently, various techniques, including optical absorption spectroscopy, Raman spectroscopy, photoluminescence spectroscopy, transient optical technology, atomic force microscopy (AFM), multi-function scanning probe microscopy, and transmission electron microscopy (TEM), etc., are widely utilized as powerful tools for fully characterize the interfacial coupling of vdWHs. Here, we will start with the general characterization techniques commonly used to characterize the interfacial coupling of vdWHs. i.e., both steady-state and transient optical characterization methods, which are discussed first in Sections 2.1 and 2.2. In addition, we will summarize some research progress of some other techniques, including SPM, TEM, etc., in Section 2.3.

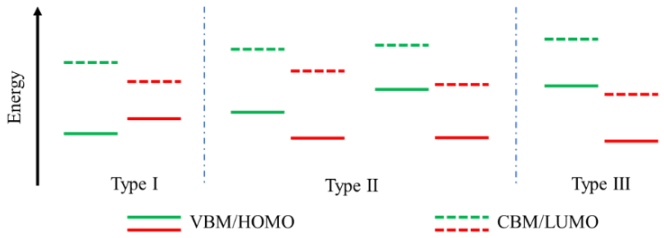

Figure 2. Schematic of type I, type II, and type III arrangements of heterostructures.

Table 1. The types of vdWHs arrangement mentioned in the review.

Heterostructures	Band-Alignment Type	Reference
$MoSe_2$/CuPc	type-II	[38]
hBN/WS_2	type-I	[39]
WS_2/$MoSe_2$	type-II	[40]
MoS_2/WSe_2	type-II	[41]
MoS_2/TaS_2	type-II	[42]
WS_2/$ReSe_2$	type-II	[43]
2L-α-In_2Se_3/1L-$MoSe_2$	type-I	[44]
Bulklike In_2Se_3/1L $MoSe_2$	type-II	[44]
MoS_2/pentacene	type-II	[36]
WS_2/MoS_2	type-II	[45]
MoS_2/PbI_2	type-I	[46]
WS_2/PbI_2	type-II	[46]
WSe_2/PbI_2	type-II	[46]
MoS_2/GaS	type-II	[47]
S3-MoSSe/InSe	type-I	[48]
Se5-MoSSe/InSe	type-II	[48]
GaTe/MoS_2	type-II	[49]

Table 1. *Cont.*

Heterostructures	Band-Alignment Type	Reference
H_2Pc/MoS_2	type-II	[50]
MoS_2/WS_2	type-II	[51]
MoS_2/ReS_2	type-I	[52]
MoS_2/WSe_2	type-II	[53]
WSe_2/C_{60}	type-II	[54]
MoS_2 and WSe_2	type-II	[55]
WS_2/graphene	type-II	[56]
MoS_2-ZnPc	type-II	[57]
WS_2/MoS_2	type-II	[58]
MXene/Blue P	type-I/type-II	[59]
phosphorene/PbI_2	type-II	[60]
$PtSe_2/ZrSe_2$	type-I/type-II	[61]
graphene/C_{60}/pentacene	type-II	[62]
$MoSe_2/WSe_2$	type-II	[63]

2.1. Steady-State Optical Characterization

In order to achieve a fundamental understanding of the interfacial coupling of vdWHs, it is essential to know the interfacial electronic structures, such as band alignment, new electronic states after interfacial coupling, defects, and so on. Moreover, the formation of high-quality atomic layers provides a perfect platform to explore intriguing physics that is not easy to observe in other systems. For instance, the stable formation of biexciton, dark excitions, and trions at room temperature have been reported in some vdWHs [64]. In the past few years, optical absorption, PL, Raman, etc., optically related characterization techniques have proven to be very powerful tools to provide abundant information about the interfacial coupling of vdWHs, such as electronic structure, charge transfer, local strain, electron–phonon interaction, and multi-body effect, etc., at the interface [65,66]. Since these optical techniques can be easily operated under an ambient atmosphere by using advanced focusing systems together with a great laser source; however, optical spectra with high spectral resolution and high spatial resolution can be detected on vdWHs. In addition, equipped with a temperature control system, time-dependent spectra can also be obtained to provide more information about the interfacial coupling of vdWHs, such as the coupling between charge and spin, electron–phonon interactions, and order and disorder states in vdWHs. Note that sometimes ultrafast laser can also be utilized as an excitation source in some of these measurements, but CW laser or other CW light sources are utilized commonly for these measurements, so we will focus on the cases of using steady-state light sources here.

Raman spectroscopy is an effective non-destructive method used to study the atomic layer number, built-in strain, doping level, and structural defects in TMD materials [67–70]. It is also commonly used to examine film thickness and structural properties and determine if a heterostructure has been formed. First, Raman spectroscopy is commonly used to confirm the number of layers in the TMD samples. The number of layers of the TMD material is determined by the distance between the positions of the two fingerprint peaks. The corresponding number of layers can be obtained by calculating the distance of the peak positions. Lee et al. characterized single-layer and few-layer MoS_2 films by AFM and Raman spectroscopy [71]. They found that the E^1_{2g} mode frequency decreased, and the A_{1g} mode frequency increased with increasing layer thickness. This is shown in Figure 3a,b. This work illustrates that the frequency difference between the E^1_{2g} mode and the A_{1g} mode can be used as a reliable and convenient diagnostic method for the layer thickness of the MoS_2 samples. In addition, the Raman spectra can reflect the information about interfacial coupling by the appearance of new peaks or the splitting of the original peaks in the spectra. For instance, our previous work found a new Raman mode at ~1345 cm^{-1} in the $MoSe_2$/CuPc heterostructure due to the strong interfacial coupling between the two materials [38], as shown in Figure 3c. Furthermore, it is worth mentioning that Raman

characterization could evaluate the coupling strength of heterojunctions effectively and nondestructively. Moreover, the emergence of Raman modes in low wavenumber regions can also be used to characterize interfacial coupling. Lin et al. demonstrated that the Raman enhancement of the LB modes in hBN/WS_2 vdWHs is caused by component- vdWH electron–phonon coupling (EPC) mediated by interfacial coupling between the hBN and WS_2 components [39]. This work reports strong cross-dimensional coupling between layer-breathing phonons and electrons in the minority-layer WS_2 component, which can be well extended to tens to hundreds of layers of vdWH. The strength of this cross-dimensional EPC can be well reproduced in vdWHs by interfacial coupling and modulation of the interlayer bonding polarizability model. This work provides an effective method for the study of interfacial coupling and EPC in vdWHs. In addition, the quality of the $WS_2/MoSe_2$ heterostructure can be examined using Raman spectroscopy [40]. It was found that the A_{1g} mode of WS_2 was sensitive to the layer thickness and was found to be greatly enhanced, indicating the successful formation of a heterogeneous layer. In addition, Si et al. found that the E^1_{2g} mode in the heterogeneous structure is blue-shifted, and the A_{1g} mode is red-shifted compared to the pure MoS_2 in Figure 3d. The distance between the two modes decreases, which is related to the number of specimen layers and the peeling effect. This suggests that the formation of the MoS_2/WSe_2 heterostructure hinders the composite of multilayer MoS_2 nanosheets under the vdW force [41]. Furthermore, Amsterdam et al. [72] used Raman spectroscopy to study the growth direction of pentacene on different substrates. The ratio of the intensities of the two vibrational modes, B_{3g} (1597 cm^{-1}) and A_g (1533 cm^{-1}), used in the Raman spectrum, confirms that the pentacene films grown along the π-face on the hBN, while on SiO_2, they are grown along the edges perpendicular to the SiO_2 substrate. Furthermore, temperature-dependent Raman experiments can provide more information about the interlayer coupling of vdWHs. For instance, Chen et al. used the temperature dependence of PL and Raman spectra together to study the interlayer coupling and energy band structure of MoS_2/TaS_2 heterostructures [42]. The Raman results show that the interlayer coupling leads to the softening of the phonon vibrations in MoS_2/TaS_2 heterostructures. To sum up, Raman spectroscopy is a very powerful tool that is capable of determining the number of layers in the TMD samples, evaluating the coupling strength, and analyzing the coupling modes of vdWHs.

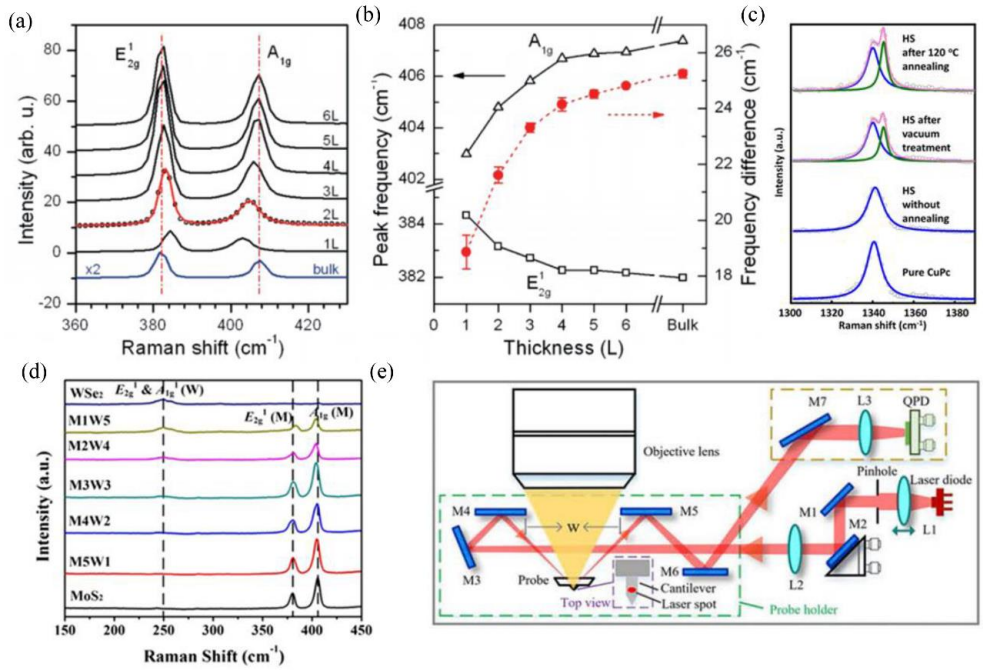

Figure 3. (**a**) Raman spectra of MoS_2 [71]. (**b**) Variation of frequencies of E^1_{2g} and A_{1g} Raman modes with layer thickness. Reprinted with the permission of Ref. [71]. Copyright 2010, American Chemical

Society. (**c**) Raman spectra of the CuPc film and $MoSe_2$/CuPc HS. Reprinted with permission from Ref. [38] Copyright 2021, American Chemical Society. (**d**) Raman spectra of MoS_2, WSe_2, and heterostructure. Reprinted with permission from Ref. [41]. Copyright 2020, Elsevier. (**e**) The diagram of OBD light path in the AFM head. Reprinted with the permission of Ref. [73]. Copyright 2022, AIP Publishing.

However, one can see that in most of the discussions above, only one characterization technique, Raman spectroscopy, was used to provide information about interfacial coupling in vdWHs. As an optical technique, the lateral resolution of Raman spectroscopy is restricted by the diffraction limit of light. Compared with Raman spectroscopy, AFM is capable of providing useful information for surface topology, physical property measurement, and manipulation with unprecedented resolution. The combination of Raman spectroscopy and AFM is considered to be a feasible solution not only to achieve both high resolution and efficiency at the same time but to provide more comprehensive information about the physical picture of the materials. The development of tip-enhanced Raman spectroscopy (TERS) is an excellent example. TERS allows the detection of weak Raman signals with nanometer spatial resolution by using a novel metal tip to provide a strong local plasma field, which is unreachable with common Raman detection [74,75]. Very recently, the Wu group has developed a novel thin head AFM that can be integrated with a Raman microscope to provide the fast and high-resolution measurement of 2D materials [73]. As far as we know, however, the reports of the applications of these techniques in the investigation of the interfacial coupling of vdWHs are rare. In the near future, it is expected that more details will be seen about the roles of the defects, absorption of environmental molecules, as well as local strain, etc., in the interfacial coupling of vdWHs by utilizing these new techniques, which will definitely broaden our understanding about the insights into vdW interfacial coupling.

It is commonly known that both PL and Raman signals can be detected simultaneously, so sometimes, what is observed in the PL measurement may also be Raman peaks; one should be careful about this. However, combining PL and Raman results can provide more information about the interfacial coupling in vdWHs. For example, the Xu group reported the unusual interfacial coupling in hBN/WSe_2/SiO_2 heterostructures by utilizing the photoluminescence excitation (PLE) mapping (shown in Figure 4a,b) [76]. They found that the hBN/WSe_2/SiO_2 structure has two PLE peaks appearing at excess energies of 130 and 98 meV than that of the WSe_2/SiO_2 sample. Two new Raman signals were found by Raman testing in the hBN/WSe_2/SiO_2 structures at 130 meV and 98 meV (as shown in Figure 4c,d), matching the corresponding peaks in the PLE intensity plots. Just as we saw, PL is also a common characterization method to reveal the electronic structure and interface states at the interface of the heterostructure. One can gain information by detecting the change of PL intensity or PL peak position in the spectrum. The interfacial charge transfer can be inferred from the PL quenching. For example, Han et al. observed photoluminescence quenching in the WS_2/$ReSe_2$ heterostructure, indicating effective interlayer charge transfer [43]. Similarly, He et al. found no PL quenching in the 2L-In_2Se_3/1L-$MoSe_2$ heterostructure by comparison, indicating that the interlayer charge transfer was not significant, suggesting that 2L In_2Se_3 and 1L $MoSe_2$ did not form a type-II energy band arrangement [44]. A heterostructure consisting of monolayer WS_2 and PTCDA films was prepared by Liu et al. [35]. The PL intensities of WS_2 and PTCDA in the heterostructure in Figure 4e are reduced by $12 \pm 5\%$ and $80 \pm 10\%$, respectively, indicating that excitons generated by PTCDA and WS_2 are free at the heterogeneous interface. The blue line in Figure 4f indicates that the MoS_2 monolayer is mainly emitted by an exciton at 654 nm, and the broad peaks at 585 nm and 680 nm appear in the pentacene films. In the MoS_2/pentacene heterostructure, the PL from the MoS_2 exciton is burst by 83% [36]. Therefore, the weakening of the PL peak intensity at the interface is a measure of whether an effective charge transfer is occurring at the interface of the heterojunction. In addition, the shift of the peak positions and the appearance of

new peaks in the PL spectrum are also very useful for evaluating the interfacial coupling of vdWHs. In Figure 4g, Tonay et al. found that the intensity of P_{MoS2} in the WS_2/MoS_2 heterostructure is 5–10 times higher than that of P_{WS2}, with a new PL peak (P_{hetero}) at 1.94 eV, and its integral intensity increases with increasing annealing time. P_{MoS2} and P_{WS2} gradually decreased after annealing. Another weak emission peak, $P_{indirect}$, appears at 1.75 eV at 3 h of annealing, and the peak position is red-shifted with the increased time. The results indicate that the enhanced interlayer coupling also has an effect on the exciton luminescence of the heterostructure, and the degree of coupling can be externally adjusted by vacuum annealing [45]. Recently, PL measurements using a polarized laser as an excitation source have been applied to study the interfacial coupling in the vdWHs. For instance, circularly polarized light with left and right spins has been used to study the interaction between electrons and phonons and to detect spin currents. Circularly polarized PL measurement has been carried out to detect valley-specific interlayer excitons, which has been proved to be a useful tool for exploring spin/valley tronic applications based on vdWHs [77,78]. In addition, based on calculating photoluminescence quantum yields, one can evaluate the quantum efficiency of vdWHs, and time-resolved photoluminescence has found that the lifetime of valley excitons in monolayer TMD in different samples ranges from a few picoseconds to several hundred picoseconds [79–82]. Except for the PL spectrum, PL mapping can visualize the observation of interlayer coupling of vdWHs. One can easily see the PL quenching effect from different regions of WS_2/PbI_2 heterostructures by comparing the contrasts of optical images and PL maps (Figure 4h,i). The WSe_2/PbI_2 region is significantly darker compared to the brighter region of monolayer WSe_2 [46]. Except for the measurement at room temperature, temperature-dependent PL measurement provides more information about the assignments of various excitons and the new electronic states generated by interfacial coupling. For example, Meng et al. reported that after annealing of GaS/MoS_2 vdWHs at 300 °C under vacuum conditions, the strong coupling interaction between the two layers leads to the changes in the positions and intensities of the emission peaks [47]. This strong coupling interaction is further confirmed by low-temperature PL measurements, i.e., the peak intensities in the spectrum of GaS/MoS_2 vdWHs decrease with increasing temperature, which is due to the thermal ionization of bound excitons to free excitons at higher temperatures.

As can be seen from the above, PL measurement is a nondestructive and powerful test method not only for characterizing defects and impurities in vdWHs quickly and easily but can explore the exciton behaviors, such as interlayer exciton, hybrid exciton, multi-body effects, etc., in vdWHs. Similar to Raman and other optical microscopic techniques, the lateral resolution of the PL measurement is also only a few hundred of nanometers due to the diffraction limit of light. In order to obtain a clearer picture of the origin of the strong interlayer coupling in vdWHs, working together with other high-resolution techniques such as TEM and AFM will be a smart choice. Introducing light into the high vacuum chamber to achieve TEM-PL/Raman as well as AFM-PL/Raman measurements simultaneously is on the road. The applications of these systems to explore the interfacial coupling in vdWHs will provide more insights into the microscopic working mechanisms, such as analyzing the local electron–phonon interaction and capturing new types of excitons and even phonons.

Absorption spectroscopy is another effective way to characterize light–matter interaction for revealing interfacial electronic coupling of vdWHs. The absorption spectrum is the spectrum of a substance that absorbs a photon and jumps from a lower energy level to a higher energy level. The absorption intensity of vdWHs is often the superposition of the absorption intensity of two materials. Guo et al. [48] found that the MoSSe monolayer has higher light absorption in the visible region, and the InSe monolayer has higher light absorption in the UV region. After the formation of vdWH, interlayer coupling occurs between the two monomolecular layers, and the reduction in the forbidden band gap produces charge transfer and enhanced light absorption. Therefore, MoSSe/InSe vdWHs have significantly improved light absorption, especially in the UV region. Similarly, as shown in Figure 5a, the optical absorption properties of $GaTe/MoS_2$ vdWH in the visible

and UV regions are significantly enhanced compared to the GaTe monolayer and MoS_2 monolayer, indicating that the coupling between the monolayers leads to the band gap reduction and charge transfer, and thus the enhancement of the light absorption [49]. It has also been noted that the absorption spectrum of a vdWH is not only a superposition of the absorption spectra of two individual layers but sometimes reflects the interfacial coupling by the appearance of new absorption peaks or the peak shift of some original peaks due to the interlayer interactions. Therefore, it can also be used to characterize the coupling at the interface of vdWHs. For example, in the 2D MoS_2/PbS heterojunction, PbS enhanced the light absorption of MoS_2 and induced the optical peaks red shift slightly, which is probably derived from the quantum confinement of the charge carrier wave functions [83]. The red shift of the absorption peak is also believed to be evidence of the interfacial charge transfers by forming strongly coupled heterostructures [84]. As shown in Figure 5b, the A and B exciton peaks of monolayer MoS_2 moved to a lower energy region after pentacene deposition, which is likely due to the formation of a depletion region in MoS_2 [36]. In addition, the absorption spectrum also shows the appearance of new absorption peaks or the suppression of the original peaks, etc. Sharma et al. investigated the interlayer interaction between $MoSe_2$ and GO by using absorption spectroscopy [85]. They found that the A and B exciton bands of $MoSe_2$ are suppressed (as shown in the inset of Figure 5c). The combination of absorption and Raman spectroscopies can also be utilized to study the interfacial coupling in organic–inorganic vdWHs. After depositing various metal-phthalocyanine (MPc) on top of MoS_2 to form a heterostructure, Amsterdam et al. systematically investigated the charge transfer in such vdWHs by using both Raman scattering and optical absorption spectroscopy [50]. It has been found that the interfacial charge transfer is sensitive to metal in the MPc molecules. Compared to Raman and PL spectroscopies, absorption spectroscopy indicates the first process of light–matter interaction and often provides a more direct description of light–matter interaction. Especially when used together with Raman and PL spectroscopies, it is capable of providing a comprehensive physical picture of interfacial coupling in vdWHs.

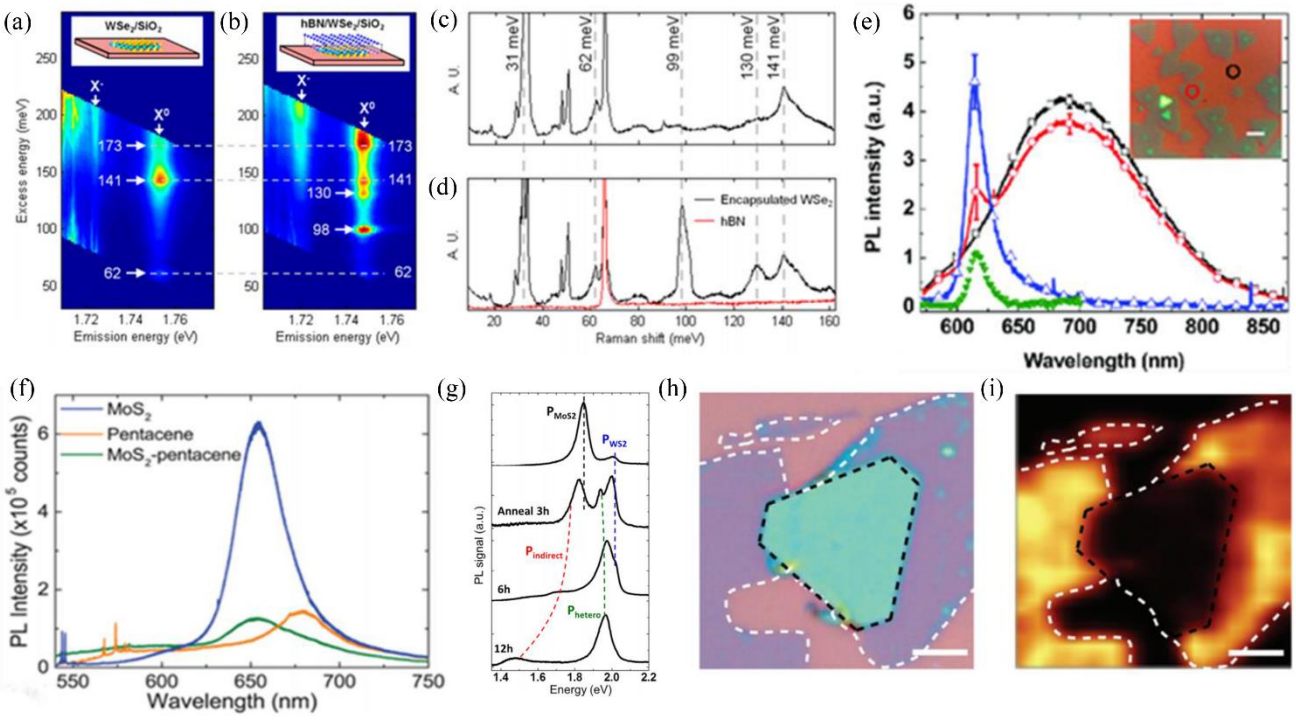

Figure 4. (**a**,**b**) PLE intensity plots of WSe_2/SiO_2 and $hBN/WSe_2/SiO_2$ [76]. (**c**) Raman spectrum of WSe_2/SiO_2 sample [76]. (**d**) Raman spectra from $hBN/WSe_2/SiO_2$ sample and hBN. Reprinted

with permission from Ref. [76] Copyright 2017, American Chemical Society. (**e**) Photoluminescence spectra of PTCDA, WS_2, and PTCDA/WS_2 Hs. The inset shows the sample under an optical microscope. Reprinted with permission from Ref. [35] Copyright 2017, American Chemical Society. (**f**) Photoluminescence spectra of MoS_2, pentacene films, and MoS_2-pentacene Hs. Reprinted with permission from Ref. [36]. Copyright 2017, American Chemical Society. (**g**) PL of WS_2/MoS_2 heterostructures after annealing. Reprinted with permission from Ref. [45]. Copyright 2014, American Chemical Society. (**h**) Optical image of WSe_2/PbI_2. [46] (**i**) The photoluminescence mapping image of the same heterostructure shown in (**h**). Reprinted with permission from Ref. [46] Copyright 2019, WILEY-VCH Verlag GmbH &. Co.kGaA.Weinheim.

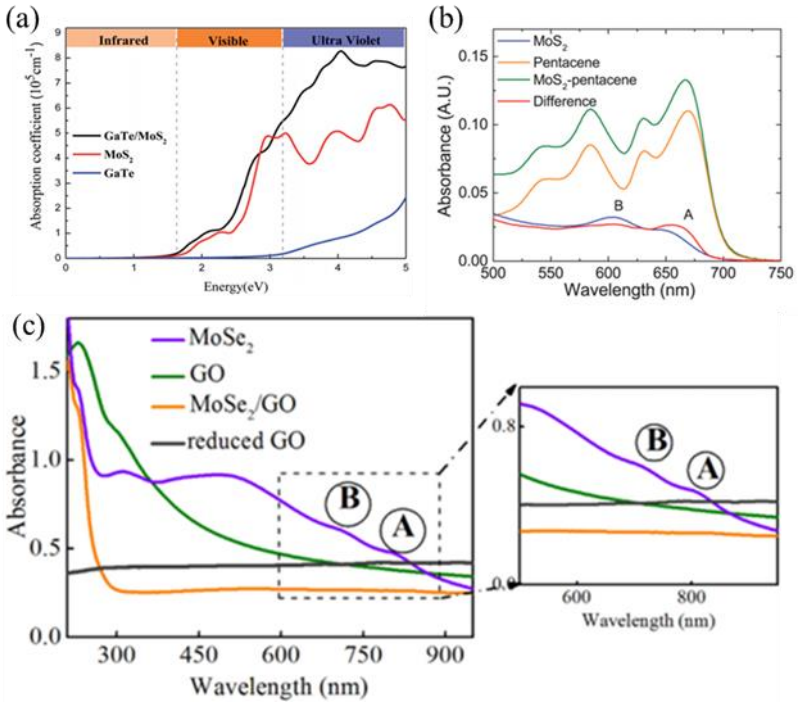

Figure 5. (**a**) Adsorption coefficients of the GaTe monolayer, MoS_2 monolayer, and GaTe/MoS_2 vdWH. Reprinted with permission from Ref. [49]. (**b**) Absorption spectra of MoS_2-pentacene heterojunction. Reprinted with permission from Ref. [36]. Copyright 2017, American Chemical Society. (**c**) Optical absorption spectra of GO, $MoSe_2$, and $MoSe_2$/GO. Reprinted with permission from Ref. [85]. Copyright 2016, APS.

In summary, we have overviewed the applications of several optical microscopy-based steady-state characterization techniques such as Raman, PL, and absorption spectroscopy in the investigation of interfacial coupling in vdWHs. In practical applications, they were sometimes used together to study the intrinsic optical properties of vdWHs to provide a comprehensive picture of the light–matter interaction process. Just as discussed above, all these techniques are limited by the lateral resolution caused by the diffraction limit of light. Therefore, how to achieve higher resolution and maintain fast and efficient tests will be the main challenges for these OM-based techniques to provide more information about the interfacial coupling of vdWHs in the future [86].

2.2. Transient Optical Characterization

The above-mentioned characterization of steady-state optics can provide information such as many-body effects, interlayer exciton formation, and local stresses, but it is difficult to directly obtain the kinetics of exciton lifetimes and other dynamics of interlayer processes such as exciton diffusion length, mobility, and optical path changes under conditions of external field excitation. In this case, transient measurements are needed. Optoelectronic processes, such as charge transfer and separation, energy transfer, and carrier lifetime at the

interface of vdWHs generally occur at the picosecond/nanosecond scale. Time-resolved photoluminescence spectroscopy (trPL) and transient absorption spectroscopy (TA) are two of the most common optical techniques to study these processes at present [18]. In addition, this paragraph also briefly introduces the time-resolved ESFG for probing time-dependent molecular conformation and interlayer electronic structure at the interfaces of vdWHs. Time-resolved photoluminescence spectroscopy is capable of providing the fluorescence lifetime by exciting the material with a short pulse of light and then recording the decay of fluorescence intensity with time. For type-II vdWHs, a staggered band alignment automatically occurs at the interface, leading to rapid charge separation of optically generated electron–hole pairs, formation of interlayer excitons, and stable trions, even at room temperature. In order to apply such vdWHs in future electronic and optoelectronics, it is necessary to achieve an overall understanding of the ultrafast carrier recovery time and the dynamics of these special excitons (interlayer excitons, biexcitons, and trions, etc.) in such a system.

The trPL spectroscopy can be used to measure carrier lifetime and confirm the formation of interlayer excitons. As shown in Figure 6a, we obtained a faster decay lifetime of 32 and 44 ps for WS_2 and $MoSe_2$, respectively, and a slower lifetime of 93 ps for the $WS_2/MoSe_2$ heterostructure derived from interlayer exciton in our previous work [40]. Okada et al. also revealed that the relaxation times of the indirect interlayer excitons are longer than direct interlayer excitons by room-temperature trPL [87], as shown in Figure 6b,c.

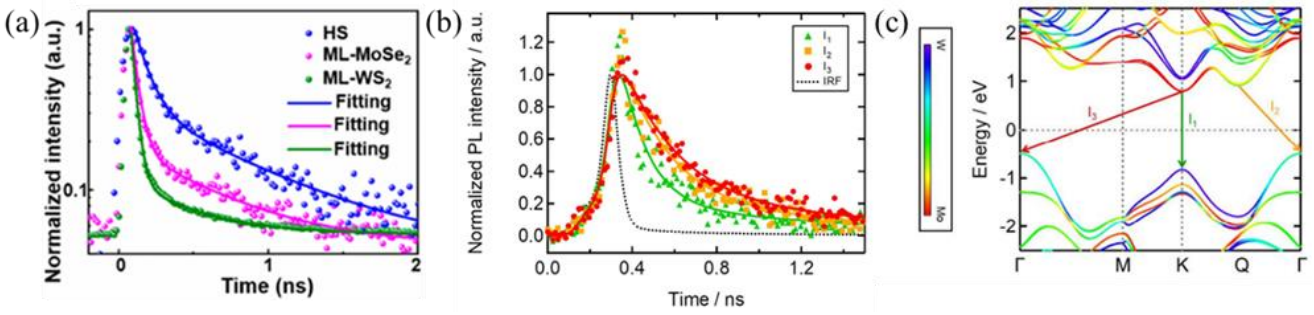

Figure 6. (**a**) Time-resolved PL decay curves for $MoSe_2$ monolayer, WS_2 monolayer, and $WS_2/MoSe_2$ Hs. Reprinted with permission from Ref. [40]. Copyright 2021, American Chemical Society. (**b**) Time-resolved PL intensity of $hBN/WS_2/MoS_2/hBN$ [87]. (**c**) DFT band structure of WS_2/MoS_2 Hs [87]. Reprinted with permission from Ref. [87]. Copyright 2018, American Chemical Society.

Transient absorption spectroscopy is also called the pump–probe technique. It is a more direct and time-resolved method of studying the photocarrier dynamics in heterostructures [88,89]. In ultrafast pump–probe experiments, two ultrashort laser pulses of different intensities and wavelengths are used, with the strong light as the pump light and the weak light as the probe light, and then both beams are focused on the same location on the sample. In the previous study, Hong et al. prepared MoS_2/WS_2 van der Waals heterostructures. By combining photoluminescence mapping with transient absorption measurements, it was determined that holes could be transferred from the photoexcited MoS_2 layer to the WS_2 layer within 50 fs [51]. In the heterostructure formed by MoS_2 and ReS_2, He et al. found that the transfer time of photocarriers was about 1 ps [52]. Peng et al. determined that in a 2D MoS_2/WSe_2 heterostructure, photocarriers injected into WSe_2 are transferred to MoS_2 within 470 fs, and the photo-generated excitons effectively dissociate into free electrons and holes and are transferred to different layers [53]. Ultrafast charge transfer has been reported at the interfaces of organic–inorganic van der Waals heterostructures. For instance, Liu et al. protonated 2DPI-graphene (2DPI-G) vdWHs and found that the generated H-2DPI- G can exhibit significant ultra-high speed charge transfer within 60 fs guided by interlayer cation-π interaction. This result can be comparable to the fastest charge transfer reported in inorganic 2D vdWHs [90]. Transient absorption spectra can also

be detected by using ultrafast white light as probe light while using monochromatic laser excitation. Homan et al. used 535 nm light as the pump wavelength and probed the sample with continuous white light (Figure 7a,b) [36]. The dissociated MoS_2 exciton was found to be transferred to the pentacene in the pentacene-MoS_2 heterostructure at a 6.7 ps time scale. The charge-separated state survives for 5.1 ns. The results show that the hole transfer rate from molybdenum disulfide to pentacene is 50%, and the remaining holes are trapped due to surface defects. This offers important prospects for the applications of such hybrid vdWHs in photovoltaics, photodetectors, and related optoelectronic techniques. Zhao et al. studied the carrier dynamics in WSe_2/C_{60} heterostructures by using 725 nm light as the pump light and continuous white light as the probe light [54]. The relevant TA spectra are shown in Figure 7c,d. By using ultrafast spectroscopy, the exciton in WSe_2 was found to be dissociated by ultrafast (~1 ps) electron transfer to C_{60} and in a nanosecond-long charge separation process. Due to the suppressed electron–hole exchange interaction after exciton dissociation, the hole in WSe_2 has a spin/valley polarization lifetime of 60 ps at room temperature, which is two orders of magnitude longer than that of the hole in an isolated WSe_2 monolayer. In addition to probing the length of carrier lifetime, the TA method can be used to purposefully excite and probe special electronic states, such as special excitons. Heterostructures formed by MLs of MoS_2 and $MoSe_2$ were studied by Ceballos et al. [91]. The formation of interlayer excitons was demonstrated by the choice of excitation and detection light, and the lifetime of interlayer excitons was fitted. As shown in Figure 7e, by probing the MoS_2 resonance and monitoring the electron density in MoS_2, it can be concluded that the charge transfer process occurs on the sub-picosecond time scale. Moreover, measurements performed on longer time scales show (Figure 7f) that indirect excitons are formed due to the separation of electrons and holes in the two layers with longer lifetimes than in MoS_2 MLs. In addition, the time-resolved pump–probe measurements have been developed. It can be used to extract the spatial diffusion length, carrier mobility, and other semiconductor-related parameters of photoexcited carriers in vdWHs. Liu et al. [92] used this technique to study the charge transfer characteristics of two heterostructures, WS_2/Bi_2O_2Se and MoS_2/Bi_2O_2Se. Time-resolved pump–probe measurements showed interlayer charge transfer with near unit transfer efficiency and formation of interlayer excitons with long, complex lifetime in these two heterostructures.

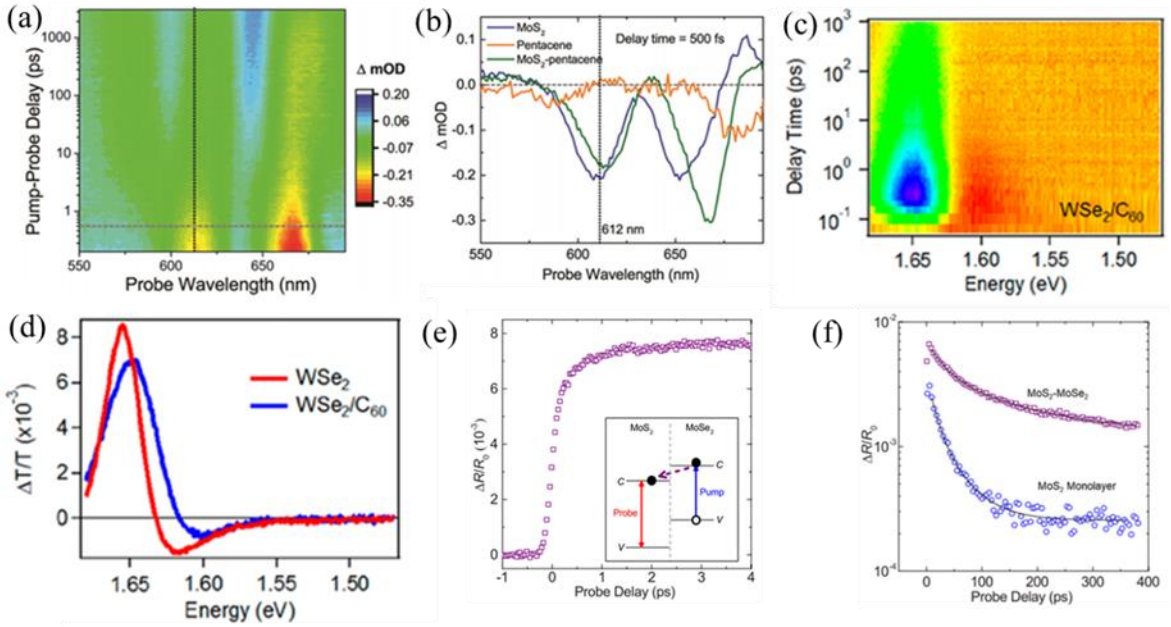

Figure 7. (**a**) Two-dimensional transient absorption spectra for the MoS_2-pentacene heterojunction [36]. (**b**) Transient absorption spectroscopy of the MoS_2-pentacene heterojunction. Reprinted

with permission from Ref. [36]. Copyright 2017, American Chemical Society. (**c**) Two-dimensional color plot of TA spectra of the WSe_2/C_{60} heterojunction [54]. (**d**) TA spectra of the WSe_2 monolayer and WSe_2/C_{60} heterojunction. Reprinted with permission from Ref. [54]. Copyright 2021, American Chemical Society. (**e**) The electron density after excitation of photocarriers in MoS_2. Built-in illustration showing pump–probe configuration. [91]. **(f)** The electron density of heterostructures and MoS_2 monolayer. Adapted with permission from Ref. [91]. Copyright 2014, American Chemical Society.

Transient absorption spectroscopy is capable of providing an ultrafast laser pump–probe detection for studying carrier dynamics such as relaxation processes in excited states and interfacial charge transfer as well as optical pathways in vdWHs. Most of the fast lasers used now are in the levels of hundreds of femtoseconds to picoseconds. However, a very important process related to the interfacial coupling in vdWHs, phonon relaxation, usually decays very fast and can hardly be captured by current measurement conditions. Therefore, the development of a faster laser will strongly promote the research progress and broaden the understanding of vdW interaction in such Hs.

In addition to the trPL and TA methods described above, second-harmonic generation (SHG) is a highly sensitive fine magnetic order probe that opens up the possibility of two-dimensional magnets for applications in nonlinear and nonreciprocal optics. Nonreciprocal second-order nonlinear optical effects appearing in bilayer CrI_3 were reported by Sun et al. [93]. It is shown that although the parent lattice of bilayer CrI_3 is centrosymmetric and does not contribute to the SHG signal, the observed giant nonreciprocal SHG originates from laminar antiferromagnetic ordering only, breaking both spatial inversion symmetry and temporal inversion symmetry. Yao et al. used ultrashort laser pulses to excite electrons and holes in the heterogeneous structure of MoS_2/WS_2 [55]. The electrons and holes are separated from the two monomolecular layers, generating an electric field that causes the incident fundamental wave to produce a second harmonic. The space charge field generated by the charge transfer decays with a time constant of 125 ps. The long-time constant is consistent with the space charge field lifetime, which is obtained from time-varying differential SHG measurements. This work provides an all-optical method for studying charge transfer with high temporal resolution. In addition, a new set of methods, i.e., sum frequency generation (SFG), electronic sum-frequency generation (ESFG) and time-resolved ESFG (TR ESFG) spectroscopies have been developed to provide interfacial molecular conformation, electronic structure and the dynamics of 2D materials [94–96]. ESFG utilizes narrow-band and broadband visible (including NIR) femtosecond pulses to provide high-quality interface-selective electron spectroscopy. TR-ESFG combines femtosecond optical excitation and ESFG measurements to provide interface-selective time-resolved electron spectroscopy to study the ultrafast dynamics of interfacial molecules [97–100]. Li et al. demonstrated that electronic sum-frequency generation (ESFG) spectroscopy could be used to determine the electronic structure of interfacial molecules at a solid/solid interface [99]. It is studied by ESFG that the conformation of P3HT at the interface of P3HT/n-doped Si (111) is more homogeneous than the native conformation. There are still rare reports of applying such techniques on both inorganic 2D/2D heterostructures and inorganic–organic vdWHs. We believe as by combining such techniques together with trPL and TA, etc., techniques, more insights about the relationship between interfacial coupling and device performance of vdWHs will be revealed.

In summary, transient spectroscopy has been rapidly developed in recent years. The development of ultrafast spectroscopy techniques has also accelerated the combination with other techniques. Some of the more common combined techniques are electron diffraction, AFM, microwave techniques, angle-resolved photoemission spectroscopy (ARPES), STM, and other techniques. The applications of these techniques will provide more insights into the interfacial coupling in vdWHs. In addition, in practical applications, in situ transient absorption spectroscopic tests and other steady-state spectroscopic experiments of vdWHs-based devices under performance will allow a better understanding of the microscopic mechanisms for nanodevices and aid in the optimization of device structures in the future.

2.3. Other Characterizations

In addition to the several optical characterization methods described above, there are some other characterization techniques, such as multi-function SPM (including KPFM, AFM, and STM), ARPES, and transmission electron microscopy (TEM), etc., have proven to be very powerful tools to study the interfacial coupling of vdWHs. Although optical methods discussed above are capable of providing a lot of useful information, especially ultrafast time resolution measurements, about the interfacial coupling of vdWHs, they are still limited in their spatial resolution since the beam size of the laser can usually be focused on a few hundred nanometers to microns. Compared to the optical methods, SPM techniques, ARPES, and TEM have a much higher spatial resolution, but a high vacuum is usually required.

KPFM can be used to provide the surface potential, local states, and working function of vdWHs. For instance, KPFM has been utilized by Huang et al. to prove that separating photogenerated holes toward ZnPc and away from the trap states in MoS_2 in MoS_2/ZnPc vdWH can effectively suppress unsolved persistent photo-conductance in as-built photodetectors [23]. Except for KPFM, electrostatic force microscopy (EFM) is also very useful for investigating the local electrical information at the surface of vdWHs, including charge distribution, carrier density, and so on [101]. For example, EFM measurements have been carried out by Jariwala et al. to confirm directly the existence of band bending in the pentacene/MoS_2 junction region, which aids in carrier separation in such vdWHs-based photovoltaics [102]. It has been noted that in the cases above, both KPFM and EFM operate under an ambient atmosphere; therefore, their spatial resolutions are largely limited by the existence of adsorbed molecules, contamination, and water films at the surface; even probes with ultrasharp tips were used during the measurements. KPFM and EFM under high vacuum enable better spatial resolution; however, the surface of the samples should be super clean, and annealing at high temperature is usually needed to achieve high vacuum conditions in the chamber. STM is also a powerful tool that can be utilized to investigate the interfacial coupling of vdWHs. Especially, ultrahigh-vacuum STM, as equipped with scanning tunneling spectroscopy (STS), can achieve the measurement of the electronic structure of vdWHs with a spatial resolution even down to the atomic level. For example, Ospina et al. found through theoretical STM images that the electronic structure of hBN/BP was found to change depending on the type of defects introduced. These defects can be identified in STM experiments even if they are located below the phosphorus layer [103]. Chiu et al. used microbeam X-ray photoelectron spectroscopy and scanning tunneling microscopy/spectroscopy to determine the energy band offsets in the transition metal dihalide heterostructures. They determined the type-II alignment between MoS_2 and WSe_2 with values of 0.83 eV and 0.76 eV for the valence band and conduction band offsets, respectively. The valence band offsets obtained from density flooding theory are in agreement with the experimental results [104]. Furthermore, combining STM and STS measurements, Parks et al. discovered that the defects in the MoS_2 can be effectively passivated by depositing TiOPc molecules on top of MoS_2 [105].

In addition, ARPES is the only experimental technique that can accurately characterize band structures in momentum space directly. This technique can distinguish clear band structures, although a high vacuum is usually required during the ARPES measurement. Aeschlimann et al. found that the lifetime of the charge separation transient in the WS_2/graphene heterostructure was close to 1 ps. They attributed this finding to spatial differences in scattered phases caused by the relative alignment of WS_2 and graphene bands revealed by high-resolution ARPES [56].

Moreover, TEM is a very powerful tool to characterize interfacial coupling in vdWHs with high spatial resolution, especially as equipped with energy spectroscopy, such as electron energy dissipation spectroscopy (EDS) and electron energy loss spectroscopy (EELS). For example, Kafle et al. determined that MoS_2 is a single crystal while ZnPc is a polycrystal in MoS_2-ZnPc heterostructures [57]. Wang et al. observed that the diameter of the WS_2/MoS_2 vdWHs nanoscroll is about 100 nm by TEM. The central region is

darker than the edge of the nanoscroll, indicating that WS_2/MoS_2 vdWHs nanoscroll has a dense scrolled structure [58]. The VSe_2/WSe_2 vdWHs were studied by Li et al. [106]. Detailed atomic structure characterization of VSe_2/WSe_2 vdWHs was performed by a combination of TEM, scanning transmission electron(STEM) microscopy, and EDS. In addition, X-ray diffraction (XRD), X-ray photoelectron spectroscopy (XPS), and four-wave mixing (FWM) spectroscopy et al. have been applied in the characterization of van der Waals heterostructures [107] to provide overall information about the interfacial coupling.

The above techniques have been commonly used to characterize the interfacial coupling of vdWHs. In most practical cases, it is hard to obtain all the information by only one technique; therefore, the combination of multiple techniques is very necessary to obtain more comprehensive information about the interfacial coupling in vdWHs. More importantly, except the development of advanced characterization techniques, new calculations methods, as well as the development of the new theory in this field, will be in urgent demand to either provide more accurate calculation results to support the experimental data or to predict the new physics in this fields in the future.

3. Modulation of Interfacial Coupling

As stated by Nobel Prize winner Herbert Kroemer, "the interface is the device" [108]. Indeed, interfaces are ubiquitous in electronic and optoelectronic devices and dominate device performance. Therefore, it is essential to gain a basic understanding of the interface, develop rational modulation methods to tune the interface effectively, and thus optimize the device structure and control the performance of devices eventually. In particular, interfacial coupling in vdWHs dominates the interfacial properties and holds a particular interest in optoelectronics. Previously, several mechanisms, such as the delocalization of electron wavefunction in momentum space [109], coherence enhancement [110], Coulomb potential enhancement [111], resonance transfer to higher energy states [109], phonon assistance [112], new mechanisms for hot electron/hot hole relaxation [113], etc., have been proposed to explain the fascinating phenomena observed in vdWHs. Meanwhile, many research groups reported that the interfacial electronic structures, such as bandgap, exciton formation, spin, etc., could be controlled experimentally by materials selection, as well as by applying external fields. Therefore, electron–hole behaviors across the vdWHs could be well tailored, either to generate photons with a designed frequency or to separate to form free carriers for photodetection or photovoltaics. Except for the material selection, various modulation methods, including interfacial strain engineering, structural optimization, and applied external fields, have been developed in the last decade to make the rational design of vdWHs-based nanodevices possible [40,114]. Herein, we overview the timely research progress in the effective approaches to modulate the interfacial coupling in vdWHs for future nanodevices. The modulation methods by applied fields, such as electric, optical, and mechanical fields and stacking angle [115], will be briefly reviewed in this section. According to these interfacial engineering methods, the interfacial properties, including carrier generation, separation, transport, and charge transfer pathways and dynamics, can be efficiently tuned.

3.1. Strain Engineering Modulation

Efficient interfacial charge transport is essential for the construction of high-performance optoelectronic devices based on vdWHs. Due to the excellent mechanical properties of 2D materials, strain engineering is considered an effective means to modulate the energy band structure of 2D materials and thus the interfacial transport of vdWHs [116]. A lot of 2D materials have high in-plane mechanical strength and very small bending stiffness, which makes them particularly suitable for strain engineering [117]. For example, monolayer MoS_2 will undergo a direct to indirect band gap transition at 2% tensile uniaxial strain and a semiconductor–metal transition at 10–15% tensile biaxial strain [118,119]. Cho et al. [117] also investigated the strain tunability of the electronic structure in the MoS_2/WSe_2 heterostructure (the sample schematic is shown in Figure 8a) by placing the

heterostructure in a wrinkled PDMS substrate. Effective strain tuning of the Γ-K interlayer excitons can be observed by applying ~107 meV/% uniaxial strain. They also found that momentum–space indirect Γ-K interlayer excitons are approximately twice that of the constituent intralayer excitons (As shown in Figure 8b). According to their results, the interlayer coupling of such vdWHs can be directly tuned in the local strain structure. Except for the experimental reports, many calculations have also been performed either to support the experimental results or to predict the modulation of strain on interfacial coupling in vdWHs too. For example, the density functional theory (DFT) calculations that have been carried out in this work to investigate the experimental observation are consistent with the calculations [120]. In addition, Guo et al. systematically evaluated the modulation of the electronic structure, optical properties, and mechanical properties of MXene/Blue P vdWHs under strain by density generalized theory [59]. It is predicted that the type-I heterostructure of Zr_2CO_2/Blue P vdWHs can be transformed into the type-II heterostructure under appropriate strain conditions, which is favorable for charge separation. These experimental and theoretical works highlight the potential of strain engineering in the interfacial coupling of vdWHs. Except for applying a tensile strain, applying high pressure directly on the vdWHs has also been carried out as an effective method to modulate the interfacial coupling in vdWHs [40,121]. In our previous work, we reported an effective modulation of interfacial coupling in high-quality $WS_2/MoSe_2$ heterostructure by applying hydrostatic pressure through diamond anvil grooves. It is interesting that the transition from intralayer excitons to interlayer excitons can be efficiently tuned under high pressure [40]. Especially, the energy of interlayer exciton in this vdWH is very stable and almost kept unchanged under high pressure (Figure 8c). Theoretical calculations also reveal that the enhanced interlayer interaction in $WS_2/MoSe_2$ heterostructure under pressure leads to enhanced interlayer exciton behavior. This work provides an effective strategy to study the interlayer interactions of vdWHs by pressure modulation. Therefore, no matter whether applying tensile strain or high pressure or placing the vdWHs on a patterned substrate, the interfacial coupling, including interfacial electronic structure, exciton formation, and even moiré potential landscape [122], can be effectively modulated. All of these results establish that strain engineering is an effective tool to tailor interfacial coupling and explore new physics of vdWHs for optoelectronics on demand [123].

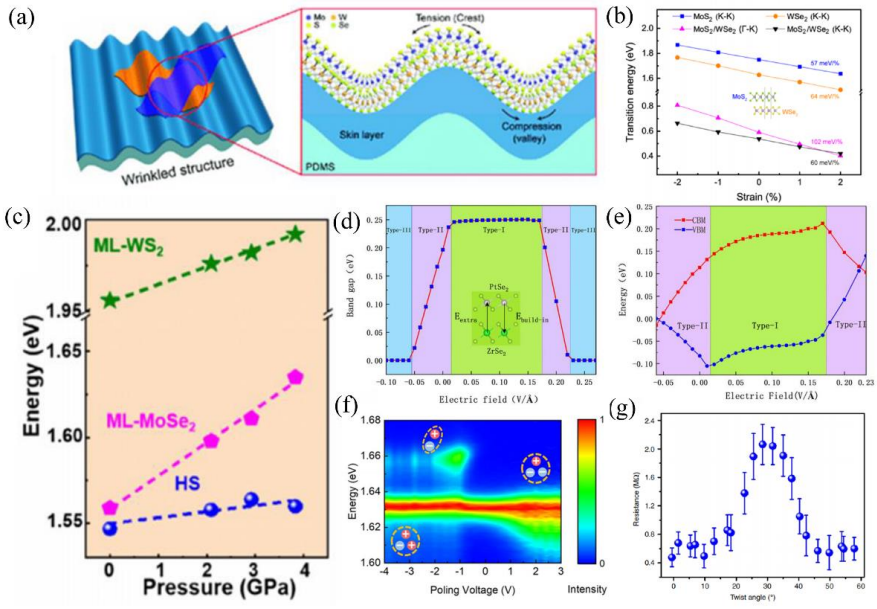

Figure 8. (**a**) Schematic diagram of the folded MoS_2/WSe_2 heterostructure [117]. (**b**) Monolayer MoS_2 and monolayer WSe_2, MoS_2/WSe_2 electron leap energy as a function of strain. The stacking order

of AB layers is shown in the inset. Reprinted with permission from Ref. [117]. Copyright 2021, American Chemical Society. (**c**) Variation of peak energy of A_{MoSe2} and A_{WS2} with pressure. Reprinted with permission from Ref. [40]. Copyright 2021, American Chemical Society. (**d**) Band gap variation of $PtSe_2/ZrSe_2$ vdWHs under different electric fields [61]. (**e**) Band edges variation of $PtSe_2/ZrSe_2$ vdWHs under different electric fields. Reprinted with permission from Ref. [61]. Copyright 2020, Elsevier. (**f**) PL spectrum of $MoSe_2$ at polarization voltages from −4V to +3V. Reprinted with permission from Ref. [124]. Copyright 2021, American Chemical Society. (**g**) Resistances of MoS_2/Gr heterostructures with different twisted angles [125].

The above research shows that after applying stress to the sample, by changing the magnitude and direction of the stress, the band gaps will change accordingly. The vdWHs properties will also be effectively tuned. Up to now, there have been few studies on the effect of strain on interlayer coupling in vdWHs. Especially, moiré potential was revealed as local lattice distortion; therefore, understanding and introducing the strain field engineering to achieve a similar effect of strong moiré potential in the interfacial coupling of vdWHs will provide guidance for the design of optoelectronic devices with an optimized performance by local stain engineering.

3.2. Electric Field Modulation

Except for strain engineering, the modulation of the interfacial coupling of vdWHs by applying an electric field has been reported as well. As early as 2009, bilayer graphene showed a significant band gap under a large electric field [126]. Similarly, the band structures of vdWHs can also be effectively adjusted under an electric field. Generally, the realization of the electronic control of interfacial coupling in vdWHs required the nanoscale control of charge doping in these materials. Theoretical predictions have been carried out by many research groups to examine the tunability of interfacial coupling in vdWHs by adding electric bias. For example, Wei et al. calculated the band gap of the phosphorene/PbI_2 heterojunction, which varied from 0 to 0.90/1.54 eV in density functional theory with applied electric field [60]. In addition, some research groups examined the electric effect on vdWHs by using STM or conductive AFM tips or SEM electron beams [114,127]. These methods benefit from having no contaminations from the complicated device fabrication processes; thus, they are perfect for the experimental exploration of electrical control in vdWHs. For instance, the Crommie group achieved a nanoscale visualization of the electrical doping of graphene/boron nitride vdWHs by using an STM tip [127]. Some attempts have also been made to obtain effective nanoscale doping in 2D materials by using focused electron-beam irradiation in SEM [114,128]. In 2020, the Zettl group reported a fully reversible high-resolution electron beam doping on graphene/MoS_2 vdWHs. By employing a BN-encapsulated geometry, direct electron-beam irradiation could be effectively avoided, and the doped vdWHs demonstrated a previously inaccessible regime of high carrier concentration and high mobility, even at room temperature [114]. Although these techniques offer an efficient route for tailoring the doping in vdWHs at the nanoscale, they are not compatible with large-scale doping operations. In order to make the approach technologically practical, the electrical-modulation methods need to be applied in higher levels of functional systems, such as logic circuits. Therefore, an FET-based device structure has been designed to evaluate the effect of electric bias on vdWHs. For instance, one can see that the relationship between the band gap/band edges of $PtSe_2/ZrSe_2$ vdW heterojunction with an external electric field in Figure 8d,e [61], which directly enhanced the versatile applications of $PtSe_2/ZrSe_2$ vdWHs in electronics and optoelectronics under an external electric field. Among these research works, FET-based device structures were usually fabricated to apply an external electric field on the vdWHs through the top gate or back gate using normal dielectrics. However, for 2D materials, it is challenging to achieve a high doping level by using normal gate dielectrics due to their atomically thin structure and limited space for the dopants with sufficient numbers without causing huge damage to the structure. Therefore, electrostatic gating, e.g., ionic liquid and some ferroelectric

substrates, have also been utilized to alter the properties of vdWHs by tuning the sign and concentration of electrical doping to a high doping level without changing the chemical compositions of the vdWHs [129,130]. Especially, along with the recent discovery of 2D ferroelectric materials, similar van der Waals structures can be built on top of 2D ferroelectric substrates [130]. Usually, the spontaneous electrical polarization of ferroelectric materials can be reversed by applying an intensified electric field; thus, it can be performed locally to create a spatial domain pattern of positive or negative polar surfaces and provides a strategy for lateral modulation in TMD to generate an electrostatic driven p-n homojunction. For example, Mao et al. found that the electric polarization of CIPS leads to continuous, large electron modulation in the monolayer $MoSe_2$ in the $MoSe_2/CuInP_2S_6$ (CIPS) 2D ferroelectric heterostructure. Using saturated ferroelectric polarization of CIPS, electron-doped or hole-doped $MoSe_2$ can be achieved in a single device (Figure 8f). These devices have non-volatile behavior for up to 3 months. The results provide a new pathway for low-power and long-time tunable optoelectronic devices [124]. Wen et al. also found that $MoSe_2$ and WSe_2 can bind to the ferroelectric lithium niobate surface and that the domain orientation of the $LiNbO_3$ has a strong effect on the TMD optoelectronic properties. Monolayer TMD sheets can be designed with underlying ferroelectric domains to create p-n homogeneous junctions that are sensitive to laser power and ambient temperature. This approach lays the foundation for creating active, electrically-driven, and controllable optoelectronic elements on a $LiNbO_3$-integrated photonic platform [131]. In summary, the external electric field can modulate the height of the Schottky barrier, the type of interfacial contact, and the number and direction of the interfacial charge transfer. It can also realize the reversible flip of the electric field at the heterostructures interface so that its optical response is continuously adjustable. Electric field modulation has thus become one of the current hot spots of research. However, up to now, there are still few reports regarding the electrostatic field regulation on organic–inorganic heterojunctions based on 2D materials and organic small molecules, except organic–inorganic hybrid perovskite [132]. Moreover, such electric field modulation is often limited by dielectric breakdown; other modulation methods are also needed to controllably tune the interfacial coupling in vdWHs.

3.3. Optical Field Modulation

Optical modulators are increasingly in demand for existing and emerging technologies, and high-performance optical modulation has become a hot topic of current research. It is significant to develop high-performance optical modulation with compact, economical, efficient, fast, and broadband optical interconnects [133]. Except for the electrical modulation, the photo-induced tuning of vdWHs was also explored in recent years [134,135]. Similar to electrical doping using voltage pulses from the STM tip [136], photo-induced doping can also be achieved through different optical excitation. The F. Wang group reported that the modulation doping of graphene could be effectively controlled through the optical excitation of BN in graphene/BN heterostructures. It is interesting to see that this photo-doping in graphene/BN is more than 1000 times stronger than that in undoped graphene/BN devices [134]. Except for the analogous modulation doping effect, strong light–matter interaction in 2D materials also triggers a lot of fascinating physical phenomena. For instance, 2D materials hold great potential to provide extremely high optical nonlinearity [137] for manipulating ultrafast light at deep subwavelengths or at the nanoscale [138], thus providing new opportunities for smaller and faster optical modulators and related devices. Optical modulation to control the strength, phase, or polarization of 2D materials has aroused more and more attention in recent years [133,139]. For example, laser pulse excitation can significantly change the carrier density, thus changing the complex refractive index of the material so as to adjust the optical response of the material to obtain better performance. Han et al. demonstrated a graphene/C_{60}/pentacene vertical heterostructure [62]. In the infrared light modulation of graphene/thin-layer C_{60} (5 nm)/pentacene, the photoresponsivity was increased from 3425 A/W to 7673 A/W. Furthermore, visible light modulation provides a tunable bandwidth from 10 to 3×10^3 Hz for tuning the in-

frared photocurrent. The introduction of vdWHs greatly enhances spectral response range and optical response, while the long lifetime of interlayer excitons and the stability at room temperature make it possible to manipulate excitons through external electric and optical fields, which opens the way for the development of new exciton devices. However, studies using light modulation to tune the interlayer interaction between two stacked 2D layers to create new material systems with strongly enhanced light–matter interactions have not been reported as far as we know. It is worth noting that for bilayer structures consisting of 2D materials with large spin–orbit coupling strengths or large inverse Rashba–Edelstein coefficients and magnetic materials, spin–charge conversion can be achieved by microwave excitation of the magnetron on the magnetic substrate, such as graphene-YIG [140] and MoS_2-YIG [141].

3.4. "Twisted Angle" Modulation

Except for the modulation by applying external fields discussed above, the properties of vdWHs can also be tuned by stacking methods. When two different monolayer materials are contacted to form a bilayer, electrons are trapped by spatially periodic "moiré potential" and can no longer move freely along the atomic plane. At the very beginning, moiré potentials have been predicted to modify the physical properties of such a bilayer. Inspired by the discovery of "magic angle" in bilayer graphene [142,143], the interlayer coupling of various van der Waals heterojunctions was also found to be effectively tuned by adjusting the twisted angle of the two monolayers of the materials since moiré potential can be different as the layers have different orientations. "Magic angle" can achieve superb electrical properties without changing the material, only by changing the external force. Therefore, tremendous reports have been published about the exploration of new physics such as unconventional superconductivity, moiré excitons, tunneling conductivity, nonlinear optics, structural super lubrication, and so on, in 2D systems by tuning the twisted angle in the past few years [144–148]. It has been noted that there are many review papers discussing the "magic angle" in bilayer graphene [142,149]; therefore, we will only focus on the modulation of the interfacial coupling in van der Waals heterostructures formed by TMD materials and graphene by twisted angle.

Similar to the "magic angle" effect in bilayer graphene, Liao et al. found that the vertical electric conductivity behavior of MoS_2/graphene heterostructures strongly depends on the stacking angle of the heterostructure, and its vertical conductivity increases monotonically with the stacking angle from 0° to 30°. The vertical conductivity of a 30° stacking angle heterostructure is approximately five times higher than that of a 0° stacking angle. (As shown in Figure 8g) Density functional theory (DFT) simulations suggest that such variation in conductivity arises from the difference in transmission coefficients of heterostructures with different twist angles [125]. In addition, studies have also shown great opportunities for modulation of the optical properties of vdWHs by changing the twisted angle of two monolayer materials. Cao et al. discovered that when two parallel graphene layers are stacked at a delicate angle of about 1.1°, a superconducting effect occurs. It shows that twisted bilayer graphene is an ideal material for studying strongly correlated phenomena [142,143]. They subsequently discovered moiré superconductors in magic-angle twisted trilayer graphene, and the tunability of this system in terms of electronic structure and superconductivity properties is superior to that of magic-angle twisted bilayer graphene [150]. They further investigated the broken symmetry many-body ground state of magic-angle twisted bilayer graphene and its nontrivial topology using thermodynamic and transport measurements. The importance of favoring Hund's coupling in the many-body ground state is demonstrated [151]. Seyler et al. report experimental evidence of interlayer valley excitons captured in moiré potentials in $MoSe_2/WSe_2$ heterostructure. This work provides an opportunity to control the two-dimensional moiré optics by varying the twist angle [63]. Similarly, Alexeev et al. demonstrated through the heterostructure of $MoSe_2/WS_2$ that exciton energy bands can hybridize, leading to resonant enhancement of the moiré superlattice effect. For heterostructures with single-molecule

layer pairs in close alignment, resonant mixing of electronic states leads to a significant effect of geometrically patterned moiré of the heterostructure on the dispersion and spectrum of hybridized excitons [147].

However, there are many problems with the means of "twisted angle" modulation. For example, the unevenness of two-dimensional materials at the atomic level can lead to multiple interfacial unevenness after stacking of bilayers or more, and the effect of this situation is amplified in heterostructures. Second, it is difficult to achieve precise control of the angle when modulating the angle of bilayer or multilayer 2D materials, while the effect on the performance of the heterostructures is unknown. Finally, the control of small angles is difficult, and how to control the angle of the torsion angle in a stable and simple way is a problem that needs to be overcome in the near future.

In conclusion, the charge and energy transfer in vdWHs is mainly determined by the energy band alignment and is also greatly influenced by the dielectric function, stacking method, crystal orientation, and external fields such as electric/optical/magnetic. Therefore, the modulation of interfacial coupling by using strain engineering, electric field, optical field, as well as changing stacking angle will provide various methods for applications of vdWHs in ultrafast and high-performance optoelectronic devices eventually.

4. Conclusions

In summary, this paper discusses the characterization and modulation methods of interfacial coupling at vdWHs. For steady-state characterization, it is generally believed that if the vdWHs have strong interlayer coupling, the Raman, absorption, and PL peaks will shift, even appearing as new peaks, and the PL strength will be quenched due to the emergence of the interlayer exciton. Further by TRPL, TA, Pump–probe spectroscopy, etc., the transient characterization can obtain the ultrafast dynamics of the interfacial molecules directly, such as the kinetics of exciton lifetimes, exciton diffusion length, carrier mobility, and so on. Of course, SHG, KPFM, TRESFG, ARPES, and other characterization methods also play an important role in verifying interlayer coupling. However, the in situ characterization of heterostructure-based devices is still rare; therefore, developing an accurate characterization technique to provide an in situ characterization of interfacial coupling in vdWH-based nanodevices under performance is essential and necessary. In addition, modulation strategies of interfacial coupling, including electrical, optical, mechanical fields, and the twisted angle between two layers, are very significant in optimizing the physical properties and thus improve the device performance based on vdWHs.

Except for the experimental work, a lot of calculation research was carried out simultaneously to predict or support the experimental results in this field. For instance, Xia et al. calculated the electronic band structure of the $WSe_2/MoSe_2$ heterostructures as a function of pressure by density functional theory with Perdew–Burke–Ernzerhof potential and obtained good agreement with the experiments [121]. Li et al. used first-principles calculations to predict that the MoS_2/SnS heterostructure was a stable interface and that a small band gap (about 0.29 eV) could absorb the entire visible region [152]. Considering most of the heterojunctions mentioned in this paper are based on 2D inorganic-null models, we believe that the characterization and modulation of organic–inorganic heterojunctions are also worth exploring experimentally and theoretically. In addition, new phenomena generated by interlayer coupling need more theoretical calculations to predict. Moreover, it is also very important to integrate 2D materials and heterojunctions into industry for practical applications.

Author Contributions: Y.W. and X.Z. initiate the whole idea about this review paper, and edit the manuscript; K.Z., S.F., Z.B., Q.M. and M.H. conduct primary literature investigation; K.Z. and D.H. prepare draft writing and edit the manuscript as well. All authors have read and agreed to the published version of the manuscript.

Funding: This work was supported by the Fundamental Research Funds for the Central Universities+2021RC203, the National Natural Science Foundation of China (Grant Nos. 11974088, 61875236, 61905010, and 61975007) and the Beijing Natural Science Foundation (Grant No. Z190006).

Institutional Review Board Statement: Not applicable.

Informed Consent Statement: Not applicable.

Data Availability Statement: Not applicable.

Conflicts of Interest: The authors declare no conflict of interest.

References

1. Li, S.; Ma, Y.; Ouedraogo, N.A.N.; Liu, F.; You, C.; Deng, W.; Zhang, Y. p-/n-Type modulation of 2D transition metal dichalcogenides for electronic and optoelectronic devices. *Nano Res.* **2021**, *15*, 123–144. [CrossRef]
2. Butler, S.Z.; Hollen, S.M.; Cao, L.; Cui, Y.; Gupta, J.A.; Gutie´rrez, H.R.; Heinz, T.F.; Hong, S.S.; Huang, J.; Ismach, A.F.; et al. Progress, Challenges, and Opportunities in Two-Dimensional Materials Beyond Graphene. *ACS Nano* **2013**, *7*, 2898–2926. [CrossRef] [PubMed]
3. Xu, M.; Liang, T.; Shi, M.; Chen, H.J.C.R. Graphene-like two-dimensional materials. *Chem. Rev.* **2013**, *113*, 3766–3798. [CrossRef] [PubMed]
4. Mak, K.F.; Lee, C.; Hone, J.; Shan, J.; Heinz, T.F.J.P.R.L. Atomically thin MoS_2: A new direct-gap semiconductor. *Phys. Rev. Lett.* **2010**, *105*, 136805. [CrossRef]
5. Georgiou, T.; Jalil, R.; Belle, B.D.; Britnell, L.; Gorbachev, R.V.; Morozov, S.V.; Kim, Y.J.; Gholinia, A.; Haigh, S.J.; Makarovsky, O.; et al. Vertical field-effect transistor based on graphene-WS_2 heterostructures for flexible and transparent electronics. *Nat. Nanotechnol.* **2013**, *8*, 100–103. [CrossRef] [PubMed]
6. Choi, J.M.; Jang, H.Y.; Kim, A.R.; Kwon, J.D.; Kim, Y.J.N. Ultra-flexible and rollable 2D-MoS_2/Si heterojunction-based near-infrared photodetector via direct synthesis. *Nanoscale* **2021**, *13*, 672–680. [CrossRef] [PubMed]
7. Nai, R.R.; Blake, P.; Grigorenko, A.N.; Novoselov, K.S.; Booth, T.J.; Stauber, T.; Peres, N.M.R.; Geim, A.K. Fine Structure Constant Defines Visual Transparency of Graphene. *Science* **2008**, *320*, 1308.
8. Zheng, W.; Liu, X.; Xie, J.; Lu, G.; Zhang, J. Emerging van der Waals junctions based on TMDs materials for advanced gas sensors. *Coord. Chem. Rev.* **2021**, *447*, 214151. [CrossRef]
9. Prabhu, P.; Jose, V.; Lee, J.M.J.M. Design Strategies for Development of TMD-Based Heterostructures in Electrochemical Energy Systems. *Matter* **2020**, *2*, 526–553. [CrossRef]
10. Liu, Y.; Weiss, N.O.; Duan, X.; Cheng, H.-C.; Huang, Y.; Duan, X. Van der Waals heterostructures and devices. *Nat. Rev. Mater.* **2016**, *1*, 16042. [CrossRef]
11. Chhowalla, M.; Jena, D.; Zhang, H. Two-dimensional semiconductors for transistors. *Nat. Rev. Mater.* **2016**, *1*, 16052. [CrossRef]
12. Iannaccone, G.; Bonaccorso, F.; Colombo, L.; Fiori, G. Quantum engineering of transistors based on 2D materials heterostructures. *Nat. Nanotechnol.* **2018**, *13*, 183–191. [CrossRef]
13. Jariwala, D.; Sangwan, V.K.; Lauhon, L.J.; Marks, T.J.; Hersam, M.C. Emerging Device Applications for Semiconducting Two-Dimensional Transition Metal Dichalcogenides. *ACS Nano* **2014**, *8*, 1102–1120. [CrossRef]
14. Cui, X.; Lee, G.H.; Kim, Y.D.; Arefe, G.; Huang, P.Y.; Lee, C.H.; Chenet, D.A.; Zhang, X.; Wang, L.; Ye, F.; et al. Multi-terminal transport measurements of MoS_2 using a van der Waals heterostructure device platform. *Nat. Nanotechnol.* **2015**, *10*, 534–540. [CrossRef] [PubMed]
15. Mak, K.F.; Shan, J. Photonics and optoelectronics of 2D semiconductor transition metal dichalcogenides. *Nat. Photonics* **2016**, *10*, 216–226. [CrossRef]
16. Novoselov, K.S.; Mishchenko, A.; Carvalho, A.; Castro Neto, A.H. 2D materials and van der Waals heterostructures. *Science* **2016**, *353*, aac9439. [CrossRef]
17. Bae, S.H.; Kum, H.; Kong, W.; Kim, Y.; Choi, C.; Lee, B.; Lin, P.; Park, Y.; Kim, J. Integration of bulk materials with two-dimensional materials for physical coupling and applications. *Nat. Mater.* **2019**, *18*, 550–560. [CrossRef]
18. Fu, S.; Qin, L.; Zhang, X.; Wang, R.; Tang, D.; Qiu, X. Interfacial optoelectronic process in organic-inorganic van der Waals hetero-structure. *Chin. Sci. Bull.* **2018**, *64*, 393–410. [CrossRef]
19. Geim, A.K.; Grigorieva, I.V. Van der Waals heterostructures. *Nature* **2013**, *499*, 419–425. [CrossRef]
20. Benka, S.G. Two-dimensional atomic crystals. *Phys. Today* **2005**, *58*, 9. [CrossRef]
21. Liu, Z.; Song, L.; Zhao, S.; Huang, J.; Ma, L.; Zhang, J.; Lou, J.; Ajayan, P.M. Direct growth of graphene/hexagonal boron nitride stacked layers. *Nano. Lett.* **2011**, *11*, 2032–2037. [CrossRef] [PubMed]
22. Gobbi, M.; Orgiu, E.; Samori, P. When 2D Materials Meet Molecules: Opportunities and Challenges of Hybrid Organic/Inorganic van der Waals Heterostructures. *Adv. Mater.* **2018**, *30*, e1706103. [CrossRef] [PubMed]
23. Huang, Y.; Zhuge, F.; Hou, J.; Lv, L.; Luo, P.; Zhou, N.; Gan, L.; Zhai, T. Van der Waals Coupled Organic Molecules with Monolayer MoS_2 for Fast Response Photodetectors with Gate-Tunable Responsivity. *ACS Nano.* **2018**, *12*, 4062–4073. [CrossRef]
24. Lou, Z.; Liang, Z.; Shen, G. Photodetectors based on two dimensional materials. *J. Semicond.* **2016**, *37*, 91001. [CrossRef]

25. Xie, C.; Mak, C.; Tao, X.; Yan, F. Photodetectors Based on Two-Dimensional Layered Materials Beyond Graphene. *Adv. Funct. Mater.* **2017**, *27*, 1603886. [CrossRef]
26. Wang, Q.; Wen, Y.; Cai, K.; Cheng, R.; Yin, L.; Zhang, Y.; Li, I.; Wang, Z.; Wang, F.; Wang, F.; et al. Nonvolatile infrared memory in MoS_2/PbS van der Waals heterostructures. *Sci. Adv.* **2018**, *4*, eaap7916. [CrossRef] [PubMed]
27. Lee, D.; Hwang, E.; Lee, Y.; Choi, Y.; Kim, J.S.; Lee, S.; Cho, J.H. Multibit MoS_2 Photoelectronic Memory with Ultrahigh Sensitivity. *Adv. Mater.* **2016**, *28*, 9196–9202. [CrossRef] [PubMed]
28. Pak, J.; Jang, J.; Cho, K.; Kim, T.Y.; Kim, J.K.; Song, Y.; Hong, W.K.; Min, M.; Lee, H.; Lee, T. Enhancement of photodetection characteristics of MoS_2 field effect transistors using surface treatment with copper phthalocyanine. *Nanoscale* **2015**, *7*, 18780–18788. [CrossRef]
29. Yun, J.-M.; Noh, Y.-J.; Yeo, J.-S.; Go, Y.-J.; Na, S.-I.; Jeong, H.-G.; Kim, J.; Lee, S.; Kim, S.-S.; Koo, H.Y.; et al. Efficient work-function engineering of solution-processed MoS_2 thin-films for novel hole and electron transport layers leading to high-performance polymer solar cells. *J. Mater. Chem. C* **2013**, *1*, 3777–3783. [CrossRef]
30. Fontana, M.; Deppe, T.; Boyd, A.K.; Rinzan, M.; Liu, A.Y.; Paranjape, M.; Barbara, P. Electron-hole transport and photovoltaic effect in gated MoS2 Schottky junctions. *Sci. Rep.* **2013**, *3*, 1634. [CrossRef]
31. Meric, I.; Dean, C.; Young, A.; Hone, J.; Kim, P.; Shepard, K.L. Graphene field-effect transistors based on boron nitride gate dielectrics. *Proc. IEEE* **2013**, *101*, 1609–1619. [CrossRef]
32. Buscema, M.; Groenendijk, D.J.; Steele, G.A.; van der Zant, H.S.; Castellanos-Gomez, A. Photovoltaic effect in few-layer black phosphorus PN junctions defined by local electrostatic gating. *Nat. Commun.* **2014**, *5*, 4651. [CrossRef] [PubMed]
33. Chen, W.; Qi, D.-C.; Huang, H.; Gao, X.; Wee, A.T.S. Organic-Organic Heterojunction Interfaces: Effect of Molecular Orientation. *Adv. Funct. Mater.* **2011**, *21*, 410–424. [CrossRef]
34. Huang, Y.; Zheng, W.; Qiu, Y.; Hu, P. Effects of Organic Molecules with Different Structures and Absorption Bandwidth on Modulating Photoresponse of MoS_2 Photodetector. *ACS Appl. Mater. Interfaces* **2016**, *8*, 23362–23370. [CrossRef]
35. Liu, X.; Gu, J.; Ding, K.; Fan, D.; Hu, X.; Tseng, Y.W.; Lee, Y.H.; Menon, V.; Forrest, S.R. Photoresponse of an Organic Semiconductor/Two-Dimensional Transition Metal Dichalcogenide Heterojunction. *Nano. Lett.* **2017**, *17*, 3176–3181. [CrossRef] [PubMed]
36. Bettis Homan, S.; Sangwan, V.K.; Balla, I.; Bergeron, H.; Weiss, E.A.; Hersam, M.C. Ultrafast Exciton Dissociation and Long-Lived Charge Separation in a Photovoltaic Pentacene-MoS_2 van der Waals Heterojunction. *Nano. Lett.* **2017**, *17*, 164–169. [CrossRef] [PubMed]
37. Huang, Y.L.; Zheng, Y.J.; Song, Z.; Chi, D.; Wee, A.T.S.; Quek, S.Y. The organic-2D transition metal dichalcogenide heterointerface. *Chem. Soc. Rev.* **2018**, *47*, 3241–3264. [CrossRef]
38. Fu, S.; Wang, R.; Tang, D.; Zhang, X.; He, D. Directly Probing Interfacial Coupling in a Monolayer $MoSe_2$ and CuPc Heterostructure. *ACS Appl Mater Interfaces* **2021**, *13*, 18372–18379. [CrossRef]
39. Lin, M.L.; Zhou, Y.; Wu, J.B.; Cong, X.; Liu, X.L.; Zhang, J.; Li, H.; Yao, W.; Tan, P.H. Cross-dimensional electron-phonon coupling in van der Waals heterostructures. *Nat. Commun.* **2019**, *10*, 2419. [CrossRef]
40. Ma, X.; Fu, S.; Ding, J.; Liu, M.; Bian, A.; Hong, F.; Sun, J.; Zhang, X.; Yu, X.; He, D. Robust Interlayer Exciton in WS_2/$MoSe_2$ van der Waals Heterostructure under High Pressure. *Nano Lett* **2021**, *21*, 8035–8042. [CrossRef]
41. Si, K.; Ma, J.; Lu, C.; Zhou, Y.; He, C.; Yang, D.; Wang, X.; Xu, X. A two-dimensional MoS_2/WSe_2 van der Waals heterostructure for enhanced photoelectric performance. *Appl. Surf. Sci.* **2020**, *507*, 145082. [CrossRef]
42. Chen, M.; Zhou, B.; Wang, F.; Xu, L.; Jiang, K.; Shang, L.; Hu, Z.; Chu, J. Interlayer coupling and the phase transition mechanism of stacked MoS2/TaS2 heterostructures discovered using temperature dependent Raman and photoluminescence spectroscopy. *RSC Adv.* **2018**, *8*, 21968–21974. [CrossRef]
43. Han, X.; He, D.; Zhang, L.; Hao, S.; Liu, S.; Fu, J.; Miao, Q.; He, J.; Wang, Y.; Zhao, H. Type-II WS2–ReSe2 heterostructure and its charge-transfer properties. *J. Mater. Res.* **2019**, *35*, 1417–1423. [CrossRef]
44. He, J.; Li, T.; Zhang, L.; He, D.; Wang, Y.; Ding, H.; Pan, N.; Zhao, H. Efficient Energy Transfer in In2Se3-MoSe2 van der Waals Heterostructures. *ACS Omega* **2018**, *3*, 11930–11936. [CrossRef] [PubMed]
45. Tongay, S.; Fan, W.; Kang, J.; Park, J.; Koldemir, U.; Suh, J.; Narang, D.S.; Liu, K.; Ji, J.; Li, J.; et al. Tuning interlayer coupling in large-area heterostructures with CVD-grown MoS_2 and WS_2 monolayers. *Nano. Lett.* **2014**, *14*, 3185–3190. [CrossRef] [PubMed]
46. Sun, Y.; Zhou, Z.; Huang, Z.; Wu, J.; Zhou, L.; Cheng, Y.; Liu, J.; Zhu, C.; Yu, M.; Yu, P.; et al. Band Structure Engineering of Interfacial Semiconductors Based on Atomically Thin Lead Iodide Crystals. *Adv. Mater.* **2019**, *31*, e1806562. [CrossRef] [PubMed]
47. Meng, X.; Chen, S.; Fang, Y.; Kou, J. Annealing-enhanced interlayer coupling interaction in GaS/MoS_2 heterojunctions*. *Chin. Phys. B* **2019**, *28*, 078101. [CrossRef]
48. Guo, Y.H.; Wang, J.L.; Hu, G.C.; Yuan, X.B.; Ren, J.F. Strain-tunable electronic and optical properties of novel MoSSe/InSe van der Waals heterostructures. *Phys. Lett. A* **2021**, *404*, 127395. [CrossRef]
49. Li, Y.; Liu, J.; Zhao, X.; Yuan, X.; Hu, G.; Yuan, X.; Ren, J. Strain forces tuned the electronic and optical properties in GaTe/MoS_2 van der Waals heterostructures. *RSC Adv.* **2020**, *10*, 25136–25142. [CrossRef]
50. Amsterdam, S.H.; Stanev, T.K.; Zhou, Q.; Lou, A.J.; Bergeron, H.; Darancet, P.; Hersam, M.C.; Stern, N.P.; Marks, T.J. Electronic Coupling in Metallophthalocyanine-Transition Metal Dichalcogenide Mixed-Dimensional Heterojunctions. *ACS Nano.* **2019**, *13*, 4183–4190. [CrossRef]

51. Hong, X.; Kim, J.; Shi, S.F.; Zhang, Y.; Jin, C.; Sun, Y.; Tongay, S.; Wu, J.; Zhang, Y.; Wang, F. Ultrafast charge transfer in atomically thin MoS_2/WS_2 heterostructures. *Nat. Nanotechnol.* **2014**, *9*, 682–686. [CrossRef] [PubMed]
52. He, J.; Kumar, N.; Bellus, M.Z.; Chiu, H.Y.; He, D.; Wang, Y.; Zhao, H. Electron transfer and coupling in graphene-tungsten disulfide van der Waals heterostructures. *Nat. Commun.* **2014**, *5*, 5622. [CrossRef] [PubMed]
53. Peng, B.; Yu, G.; Liu, X.; Liu, B.; Liang, X.; Bi, L.; Deng, L.; Sum, T.C.; Loh, K.P. Ultrafast charge transfer in MoS_2/WSe_2 p–n Heterojunction. *2D Materials* **2016**, *3*, 025020. [CrossRef]
54. Zhao, C.; Tao, W.; Chen, Z.; Zhou, H.; Zhang, C.; Lin, J.; Zhu, H. Ultrafast Electron Transfer with Long-Lived Charge Separation and Spin Polarization in WSe_2/C_{60} Heterojunction. *J. Phys. Chem. Lett.* **2021**, *12*, 3691–3697. [CrossRef] [PubMed]
55. Yao, P.; He, D.; Zereshki, P.; Wang, Y.; Zhao, H. Nonlinear optical effect of interlayer charge transfer in a van der Waals heterostructure. *Appl. Phys. Lett.* **2019**, *115*, 263103. [CrossRef]
56. Aeschlimann, S.; Rossi, A.; Chávez-Cervantes, M.; Krause, R.; Arnoldi, B.; Stadtmüller, B.; Aeschlimann, M.; Forti, S.; Fabbri, F.; Coletti, C.; et al. Direct evidence for efficient ultrafast charge separation in epitaxial WS_2/graphene heterostructures. *Sci. Adv.* **2020**, *6*, eaay0761. [CrossRef]
57. Kafle, T.R.; Kattel, B.; Lane, S.D.; Wang, T.; Zhao, H.; Chan, W.L. Charge Transfer Exciton and Spin Flipping at Organic-Transition-Metal Dichalcogenide Interfaces. *ACS Nano.* **2017**, *11*, 10184–10192. [CrossRef]
58. Wang, L.; Yue, Q.; Pei, C.; Fan, H.; Dai, J.; Huang, X.; Li, H.; Huang, W. Scrolling bilayer WS_2/MoS_2 heterostructures for high-performance photo-detection. *Nano. Res.* **2020**, *13*, 959–966. [CrossRef]
59. Guo, Z.; Miao, N.; Zhou, J.; Sa, B.; Sun, Z. Strain-mediated type-I/type-II transition in MXene/Blue phosphorene van der Waals heterostructures for flexible optical/electronic devices. *J. Mater. Chem. C* **2017**, *5*, 978–984. [CrossRef]
60. Wei, Y.; Wang, F.; Zhang, W.; Zhang, X. The electric field modulation of electronic properties in a type-II phosphorene/PbI_2 van der Waals heterojunction. *Phys. Chem. Chem. Phys.* **2019**, *21*, 7765–7772. [CrossRef]
61. Zhao, X.; Niu, W.; Zhang, H.; Dai, X.; Wei, S.; Yang, L. Effects of interlayer coupling and electric field on the electronic properties of $PtSe_2/ZrSe_2$ van der Waals heterojunctions. *Appl. Surf. Sci.* **2020**, *510*, 145316. [CrossRef]
62. Han, J.; He, M.; Yang, M.; Han, Q.; Wang, F.; Zhong, F.; Xu, M.; Li, Q.; Zhu, H.; Shan, C.; et al. Light-modulated vertical heterojunction phototransistors with distinct logical photocurrents. *Light Sci. Appl.* **2020**, *9*, 167. [CrossRef] [PubMed]
63. Seyler, K.L.; Rivera, P.; Yu, H.; Wilson, N.P.; Ray, E.L.; Mandrus, D.G.; Yan, J.; Yao, W.; Xu, X. Signatures of moire-trapped valley excitons in $MoSe_2/WSe_2$ heterobilayers. *Nature* **2019**, *567*, 66–70. [CrossRef] [PubMed]
64. Xia, W.; Dai, L.; Yu, P.; Tong, X.; Song, W.; Zhang, G.; Wang, Z. Recent progress in van der Waals heterojunctions. *Nanoscale* **2017**, *9*, 4324–4365. [CrossRef] [PubMed]
65. Xu, X.; Lou, Z.; Cheng, S.; Chow, P.C.Y.; Koch, N.; Cheng, H.-M. Van der Waals organic/inorganic heterostructures in the two-dimensional limit. *Chem* **2021**, *7*, 2989–3026. [CrossRef]
66. Liu, F.; Chow, W.L.; He, X.; Hu, P.; Zheng, S.; Wang, X.; Zhou, J.; Fu, Q.; Fu, W.; Yu, P.; et al. Van der Waals p-n Junction Based on an Organic-Inorganic Heterostructure. *Adv. Funct. Mater.* **2015**, *25*, 5865–5871. [CrossRef]
67. Johari, P.; Shenoy, V.B. Tuning the Electronic Properties of Semiconducting Transition Metal Dichalcogenides by Applying Mechanical Strains. *ACS Nano.* **2012**, *6*, 5449–5456. [CrossRef]
68. Nan, H.; Wang, Z.; Wang, W.; Liang, Z.; Lu, Y.; Chen, Q.; He, D.; Tan, P.; Miao, F.; Wang, X.; et al. Strong Photoluminescence Enhancement of MoS_2 through Defect Engineering and Oxygen Bonding. *ACS Nano.* **2014**, *8*, 5738–5745. [CrossRef]
69. Kim, D.; Shin, C.; Park, J.H.; Park, J.; Kim, T. Characteristics of a type-II n-MoS_2/p-Ge van der Waals heterojunction. *Curr. Appl. Phys.* **2020**, *20*, 802–806. [CrossRef]
70. Patel, A.B.; Machhi, H.K.; Chauhan, P.; Narayan, S.; Dixit, V.; Soni, S.S.; Jha, P.K.; Solanki, G.K.; Patel, K.D.; Pathak, V.M. Electrophoretically Deposited $MoSe_2/WSe_2$ Heterojunction from Ultrasonically Exfoliated Nanocrystals for Enhanced Electrochemical Photoresponse. *ACS Appl Mater Interfaces* **2019**, *11*, 4093–4102. [CrossRef]
71. Lee, C.; Yan, H.; Brus, L.E.; Heinz, T.F.; Hone, J.; Ryu, S. Anomalous Lattice Vibrations of Single- and Few-Layer MoS_2. *ACS Nano.* **2010**, *4*, 2695–2700. [CrossRef]
72. Amsterdam, S.H.; LaMountain, T.; Stanev, T.K.; Sangwan, V.K.; Lopez-Arteaga, R.; Padgaonkar, S.; Watanabe, K.; Taniguchi, T.; Weiss, E.A.; Marks, T.J.; et al. Tailoring the Optical Response of Pentacene Thin Films via Templated Growth on Hexagonal Boron Nitride. *J. Phys. Chem. Lett.* **2021**, *12*, 26–31. [CrossRef]
73. Lu, N.; Xiao, S.; Zhang, R.; Liu, J.; Ma, L.; Wu, S. Thin head atomic force microscope for integration with optical microscope. *Rev. Sci. Instrum.* **2022**, *93*, 083702. [CrossRef] [PubMed]
74. Sonntag, M.D.; Pozzi, E.A.; Jiang, N.; Hersam, M.C.; Van Duyne, R.P. Recent Advances in Tip-Enhanced Raman Spectroscopy. *J. Phys. Chem. Lett.* **2014**, *5*, 3125–3130. [CrossRef] [PubMed]
75. Verma, P. Tip-Enhanced Raman Spectroscopy: Technique and Recent Advances. *Chem. Rev.* **2017**, *117*, 6447–6466. [CrossRef]
76. Chow, C.M.; Yu, H.; Jones, A.M.; Yan, J.; Mandrus, D.G.; Taniguchi, T.; Watanabe, K.; Yao, W.; Xu, X. Unusual Exciton-Phonon Interactions at van der Waals Engineered Interfaces. *Nano. Lett.* **2017**, *17*, 1194–1199. [CrossRef]
77. Hsu, W.T.; Lu, L.S.; Wu, P.H.; Lee, M.H.; Chen, P.J.; Wu, P.Y.; Chou, Y.C.; Jeng, H.T.; Li, L.J.; Chu, M.W.; et al. Negative circular polarization emissions from $WSe_2/MoSe_2$ commensurate heterobilayers. *Nat. Commun.* **2018**, *9*, 1356. [CrossRef] [PubMed]
78. Rivera, P.; Seyler, K.L.; Yu, H.; Schaibley, J.R.; Yan, J.; Mandrus, D.G.; Yao, W.; Xu, X. Valley-polarized exciton dynamics in a 2D semiconductor heterostructure. *Science* **2016**, *352*, 688–691. [CrossRef] [PubMed]

79. Mak, K.F.; He, K.; Shan, J.; Heinz, T.F. Control of valley polarization in monolayer MoS_2 by optical helicity. *Nat. Nanotechnol.* **2012**, *7*, 494–498. [CrossRef]
80. Yuan, H.; Bahramy, M.S.; Morimoto, K.; Wu, S.; Nomura, K.; Yang, B.-J.; Shimotani, H.; Suzuki, R.; Toh, M.; Kloc, C.; et al. Zeeman-type spin splitting controlled by an electric field. *Nat. Phys.* **2013**, *9*, 563–569. [CrossRef]
81. Korn, T.; Heydrich, S.; Hirmer, M.; Schmutzler, J.; Schüller, C. Low-temperature photocarrier dynamics in monolayer MoS_2. *Appl. Phys. Lett.* **2011**, *99*, 102109. [CrossRef]
82. van der Zande, A.M.; Huang, P.Y.; Chenet, D.A.; Berkelbach, T.C.; You, Y.; Lee, G.H.; Heinz, T.F.; Reichman, D.R.; Muller, D.A.; Hone, J.C. Grains and grain boundaries in highly crystalline monolayer molybdenum disulphide. *Nat. Mater.* **2013**, *12*, 554–561. [CrossRef] [PubMed]
83. Li, M.; Ruan, H.; Yuan, X.; Chen, Y.; Wang, X.; Liu, Y.; Lu, Z.; Hai, J. Construction of 2D MoS_2/PbS heterojunction nanocomposites with enhanced photoelectric property. *Mater. Lett.* **2018**, *212*, 82–85. [CrossRef]
84. Zhang, Y.; Xu, J.; Mei, J.; Sarina, S.; Wu, Z.; Liao, T.; Yan, C.; Sun, Z. Strongly interfacial-coupled 2D-2D TiO_2/g-C_3N_4 heterostructure for enhanced visible-light induced synthesis and conversion. *J. Hazard Mater.* **2020**, *394*, 122529. [CrossRef] [PubMed]
85. Sharma, R.; Aneesh, J.; Yadav, R.K.; Sanda, S.; Barik, A.R.; Mishra, A.K.; Maji, T.K.; Karmakar, D.; Adarsh, K.V. Strong interlayer coupling mediated giant two-photon absorption in$MoSe_2$/graphene oxide heterostructure: Quenching of exciton bands. *Phys. Rev. B* **2016**, *93*, 155433. [CrossRef]
86. Ab-Samat, H.; Kamaruddin, S. Opportunistic maintenance (OM) as a new advancement in maintenance approaches. *J. Qual. Maint. Eng.* **2014**, *20*, 98–121. [CrossRef]
87. Okada, M.; Kutana, A.; Kureishi, Y.; Kobayashi, Y.; Saito, Y.; Saito, T.; Watanabe, K.; Taniguchi, T.; Gupta, S.; Miyata, Y.; et al. Direct and Indirect Interlayer Excitons in a van der Waals Heterostructure of hBN/WS_2/MoS_2/hBN. *ACS Nano.* **2018**, *12*, 2498–2505. [CrossRef]
88. Rivera, P.; Schaibley, J.; Jones, A.; Ross, J.; Wu, S.; Aivazian, G.; Klement, P.; Seyler, K.; Clark, G.; Ghimire, N.J.N.C. Observation of long-lived interlayer excitons in monolayer $MoSe_2$–WSe_2 heterostructures. *Nat. Commun.* **2015**, *6*, 6242. [CrossRef]
89. Ceballos, F.; Zhao, H. Ultrafast Laser Spectroscopy of Two-Dimensional Materials Beyond Graphene. *Adv. Funct. Mater.* **2016**, *27*, 1604509. [CrossRef]
90. Liu, K.; Li, J.; Qi, H.; Hambsch, M.; Rawle, J.; Vazquez, A.R.; Nia, A.S.; Pashkin, A.; Schneider, H.; Polozij, M.; et al. A Two-Dimensional Polyimide-Graphene Heterostructure with Ultra-fast Interlayer Charge Transfer. *Angew. Chem. Int. Ed. Engl.* **2021**, *60*, 13859–13864. [CrossRef]
91. Ceballos, F.; Bellus, M.Z.; Chiu, H.Y.; Zhao, H. Ultrafast charge separation and indirect exciton formation in a MoS_2-$MoSe_2$ van der Waals heterostructure. *ACS Nano.* **2014**, *8*, 12717–12724. [CrossRef] [PubMed]
92. Liu, S.; He, D.; Tan, C.; Fu, S.; Han, X.; Huang, M.; Miao, Q.; Zhang, X.; Wang, Y.; Peng, H.; et al. Charge Transfer Properties of Heterostructures Formed by Bi_2O_2Se and Transition Metal Dichalcogenide Monolayers. *Small* **2022**, *18*, e2106078. [CrossRef]
93. Sun, Z.; Yi, Y.; Song, T.; Clark, G.; Huang, B.; Shan, Y.; Wu, S.; Huang, D.; Gao, C.; Chen, Z.; et al. Giant nonreciprocal second-harmonic generation from antiferromagnetic bilayer CrI_3. *Nature* **2019**, *572*, 497–501. [CrossRef] [PubMed]
94. Yamaguchi, S.; Tahara, T. Development of Electronic Sum Frequency Generation Spectroscopies and Their Application to Liquid Interfaces. *J. Phys. Chem. C* **2015**, *119*, 14815–14828. [CrossRef]
95. Xiao, M.; Joglekar, S.; Zhang, X.; Jasensky, J.; Ma, J.; Cui, Q.; Guo, L.J.; Chen, Z. Effect of Interfacial Molecular Orientation on Power Conversion Efficiency of Perovskite Solar Cells. *J. Am. Chem. Soc.* **2017**, *139*, 3378–3386. [CrossRef]
96. Li, C.; Yang, J.; Su, F.; Tan, J.; Luo, Y.; Ye, S. Conformational disorder of organic cations tunes the charge carrier mobility in two-dimensional organic-inorganic perovskites. *Nat. Commun.* **2020**, *11*, 5481. [CrossRef]
97. Arnolds, H.; Bonn, M. Ultrafast surface vibrational dynamics. *Surf. Sci. Rep.* **2010**, *65*, 45–66. [CrossRef]
98. Wan, Q.; Galli, G. First-Principles Framework to Compute Sum-Frequency Generation Vibrational Spectra of Semiconductors and Insulators. *Phys. Rev. Lett.* **2015**, *115*, 246404. [CrossRef]
99. Li, Y.; Wang, J.; Xiong, W. Probing Electronic Structures of Organic Semiconductors at Buried Interfaces by Electronic Sum Frequency Generation Spectroscopy. *J. Phys. Chem. C* **2015**, *119*, 28083–28089. [CrossRef]
100. Li, Y.; Xiang, B.; Xiong, W. Heterodyne transient vibrational SFG to reveal molecular responses to interfacial charge transfer. *J. Chem. Phys.* **2019**, *150*, 114706. [CrossRef]
101. Hussain, S.; Xu, K.; Ye, S.; Lei, L.; Liu, X.; Xu, R.; Xie, L.; Cheng, Z. Local electrical characterization of two-dimensional materials with functional atomic force microscopy. *Front. Phys.* **2019**, *14*, 33401. [CrossRef]
102. Jariwala, D.; Howell, S.L.; Chen, K.S.; Kang, J.; Sangwan, V.K.; Filippone, S.A.; Turrisi, R.; Marks, T.J.; Lauhon, L.J.; Hersam, M.C. Hybrid, Gate-Tunable, van der Waals p-n Heterojunctions from Pentacene and MoS_2. *Nano. Lett.* **2016**, *16*, 497–503. [CrossRef]
103. Ospina, D.A.; Cisternas, E.; Duque, C.A.; Correa, J.D. Electronic structure and STM images simulation of defects on hBN/black-phosphorene heterostructures: A theoretical study. *Surf. Sci.* **2018**, *669*, 95–102. [CrossRef]
104. Chiu, M.H.; Zhang, C.; Shiu, H.W.; Chuu, C.P.; Chen, C.H.; Chang, C.Y.; Chen, C.H.; Chou, M.Y.; Shih, C.K.; Li, L.J. Determination of band alignment in the single-layer MoS_2/WSe_2 heterojunction. *Nat. Commun.* **2015**, *6*, 7666. [CrossRef] [PubMed]
105. Park, J.H.; Sanne, A.; Guo, Y.; Amani, M.; Zhang, K.; Movva, H.C.P.; Robinson, J.; Javey, A.; Robertson, J.; Banerjee, S.K.; et al. Defect passivation of transition metal dichalcogenides via a charge transfer van der Waals interface. *Sci. Adv.* **2017**, *3*, e1701661. [CrossRef] [PubMed]

106. Li, J.; Yang, X.; Liu, Y.; Huang, B.; Wu, R.; Zhang, Z.; Zhao, B.; Ma, H.; Dang, W.; Wei, Z.; et al. General synthesis of two-dimensional van der Waals heterostructure arrays. *Nature* **2020**, *579*, 368–374. [CrossRef] [PubMed]
107. Li, D.; Xiong, W.; Jiang, L.; Xiao, Z.; Golgir, H.R.; Wang, M.; Huang, X.; Zhou, Y.; Lin, Z.; Song, J.; et al. Multimodal Nonlinear Optical Imaging of MoS_2 and MoS_2-Based van der Waals Heterostructures. *ACS Nano.* **2016**, *10*, 3766–3775. [CrossRef]
108. Kroemer, H. Nobel Lecture: Quasielectric fields and band offsets: Teaching electrons new tricks. *Rev. Mod. Phys.* **2001**, *73*, 783–793. [CrossRef]
109. Zhu, X.Y.; Monahan, N.R.; Gong, Z.Z.; Zhu, H.M.; Williams, K.W.; Nelson, C.A. Charge Transfer Excitons at van der Waals Interfaces. *J. Am. Chem. Soc.* **2015**, *137*, 8313–8320. [CrossRef]
110. Ceballos, F.; Ju, M.G.; Lane, S.D.; Zeng, X.C.; Zhao, H. Highly Efficient and Anomalous Charge Transfer in van der Waals Trilayer Semiconductors. *Nano. Lett.* **2017**, *17*, 1623–1628. [CrossRef]
111. Wang, H.; Bang, J.; Sun, Y.; Liang, L.; West, D.; Meunier, V.; Zhang, S.J.N.C. The role of collective motion in the ultrafast charge transfer in van der Waals heterostructures. *Nat. Commun.* **2016**, *7*, 11504. [CrossRef]
112. Ciarrocchi, A.; Unuchek, D.; Avsar, A.; Watanabe, K.; Taniguchi, T.; Kis, A. Polarization switching and electrical control of interlayer excitons in two-dimensional van der Waals heterostructures. *Nat. Photonics* **2019**, *13*, 131–136. [CrossRef] [PubMed]
113. Zhang, J.; Hong, H.; Zhang, J.; Fu, H.; You, P.; Lischner, J.; Liu, K.; Kaxiras, E.; Meng, S. New Pathway for Hot Electron Relaxation in Two-Dimensional Heterostructures. *Nano. Lett.* **2018**, *18*, 6057–6063. [CrossRef]
114. Shi, W.; Kahn, S.; Jiang, L.; Wang, S.-Y.; Tsai, H.-Z.; Wong, D.; Taniguchi, T.; Watanabe, K.; Wang, F.; Crommie, M.F.; et al. Reversible writing of high-mobility and high-carrier-density doping patterns in two-dimensional van der Waals heterostructures. *Nat. Electron.* **2020**, *3*, 99–105. [CrossRef]
115. Zheng, Z.; Zu, X.; Zhang, Y.; Zhou, W. Rational design of type-II nano-heterojunctions for nanoscale optoelectronics. *Mater. Today Phys.* **2020**, *15*, 100262. [CrossRef]
116. Roldan, R.; Castellanos-Gomez, A.; Cappelluti, E.; Guinea, F. Strain engineering in semiconducting two-dimensional crystals. *J. Phys. Condens. Matter.* **2015**, *27*, 313201. [CrossRef] [PubMed]
117. Cho, C.; Wong, J.; Taqieddin, A.; Biswas, S.; Aluru, N.R.; Nam, S.; Atwater, H.A. Highly Strain-Tunable Interlayer Excitons in MoS_2/WSe_2 Heterobilayers. *Nano. Lett.* **2021**, *21*, 3956–3964. [CrossRef]
118. Scalise, E.; Houssa, M.; Pourtois, G.; Afanas'ev, V.; Stesmans, A. Strain-induced semiconductor to metal transition in the two-dimensional honeycomb structure of MoS_2. *Nano. Res.* **2012**, *5*, 43–48. [CrossRef]
119. Asl, M.G.; Borini, S.; Kuc, A.; Heine, T. Strain-dependent modulation of conductivity in single-layer transition-metal dichalcogenides. *Phys. Rev. B* **2013**, *87*, 235434.
120. Li, X.; Jia, G.; Du, J.; Song, X.; Xia, C.; Wei, Z.; Li, J. Type-II InSe/$MoSe_2$(WSe_2) van der Waals heterostructures: Vertical strain and electric field effects. *J. Mater. Chem. C* **2018**, *6*, 10010–10019. [CrossRef]
121. Xia, J.; Yan, J.; Wang, Z.; He, Y.; Gong, Y.; Chen, W.; Sum, T.C.; Liu, Z.; Ajayan, P.M.; Shen, Z. Strong coupling and pressure engineering in WSe_2–$MoSe_2$ heterobilayers. *Nat. Phys.* **2020**, *17*, 92–98. [CrossRef]
122. Bai, Y.; Zhou, L.; Wang, J.; Wu, W.; McGilly, L.J.; Halbertal, D.; Lo, C.F.B.; Liu, F.; Ardelean, J.; Rivera, P.; et al. Excitons in strain-induced one-dimensional moire potentials at transition metal dichalcogenide heterojunctions. *Nat. Mater.* **2020**, *19*, 1068–1073. [CrossRef]
123. Liu, T.; Liu, S.; Tu, K.H.; Schmidt, H.; Chu, L.; Xiang, D.; Martin, J.; Eda, G.; Ross, C.A.; Garaj, S. Crested two-dimensional transistors. *Nat. Nanotechnol.* **2019**, *14*, 223–226. [CrossRef] [PubMed]
124. Mao, X.; Fu, J.; Chen, C.; Li, Y.; Liu, H.; Gong, M.; Zeng, H. Nonvolatile Electric Control of Exciton Complexes in Monolayer $MoSe_2$ with Two-Dimensional Ferroelectric $CuInP_2S_6$. *ACS Appl. Mater. Interfaces* **2021**, *13*, 24250–24257. [CrossRef] [PubMed]
125. Liao, M.; Wu, Z.W.; Du, L.; Zhang, T.; Wei, Z.; Zhu, J.; Yu, H.; Tang, J.; Gu, L.; Xing, Y.; et al. Twist angle-dependent conductivities across MoS_2/graphene heterojunctions. *Nat. Commun.* **2018**, *9*, 4068. [CrossRef]
126. Mak, K.F.; Lui, C.H.; Shan, J.; Heinz, T.F. Observation of an electric-field-induced band gap in bilayer graphene by infrared spectroscopy. *Phys. Rev. Lett.* **2009**, *102*, 256405. [CrossRef]
127. Velasco, J., Jr.; Ju, L.; Wong, D.; Kahn, S.; Lee, J.; Tsai, H.Z.; Germany, C.; Wickenburg, S.; Lu, J.; Taniguchi, T.; et al. Nanoscale Control of Rewriteable Doping Patterns in Pristine Graphene/Boron Nitride Heterostructures. *Nano. Lett.* **2016**, *16*, 1620–1625. [CrossRef]
128. Zhou, Y.; Jadwiszczak, J.; Keane, D.; Chen, Y.; Yu, D.; Zhang, H. Programmable graphene doping via electron beam irradiation. *Nanoscale* **2017**, *9*, 8657–8664. [CrossRef]
129. Choi, Y.; Kang, J.; Jariwala, D.; Kang, M.S.; Marks, T.J.; Hersam, M.C.; Cho, J.H. Low-Voltage Complementary Electronics from Ion-Gel-Gated Vertical Van der Waals Heterostructures. *Adv. Mater.* **2016**, *28*, 3742–3748. [CrossRef]
130. Chu, J.; Wang, Y.; Wang, X.; Hu, K.; Rao, G.; Gong, C.; Wu, C.; Hong, H.; Wang, X.; Liu, K.; et al. 2D Polarized Materials: Ferromagnetic, Ferrovalley, Ferroelectric Materials, and Related Heterostructures. *Adv. Mater.* **2021**, *33*, e2004469. [CrossRef]
131. Wen, B.; Zhu, Y.; Yudistira, D.; Boes, A.; Zhang, L.; Yidirim, T.; Liu, B.; Yan, H.; Sun, X.; Zhou, Y.; et al. Ferroelectric-Driven Exciton and Trion Modulation in Monolayer Molybdenum and Tungsten Diselenides. *ACS Nano.* **2019**, *13*, 5335–5343. [CrossRef] [PubMed]
132. Huang, H.-M.; Zhou, H.-J.; Wu, C.-R.; Zhu, Z.-W.; He, Z.-D. Modulation of strain, electric field and organic cation rotation on the band gap and electronic structures of organic-inorganic hybrid perovskite $CH_3NH_3PbI_3$. *Chin. J. Phys.* **2020**, *67*, 559–568. [CrossRef]

133. Sun, Z.; Martinez, A.; Wang, F. Optical modulators with 2D layered materials. *Nat. Photonics* **2016**, *10*, 227–238. [CrossRef]
134. Ju, L.; Velasco, J., Jr.; Huang, E.; Kahn, S.; Nosiglia, C.; Tsai, H.Z.; Yang, W.; Taniguchi, T.; Watanabe, K.; Zhang, Y.; et al. Photoinduced doping in heterostructures of graphene and boron nitride. *Nat. Nanotechnol.* **2014**, *9*, 348–352. [CrossRef] [PubMed]
135. Li, Z.; Yang, W.; Huang, M.; Yang, X.; Zhu, C.; He, C.; Li, L.; Wang, Y.; Xie, Y.; Luo, Z.; et al. Light-triggered interfacial charge transfer and enhanced photodetection in CdSe/ZnS quantum dots/MoS_2 mixed-dimensional phototransistors. *Opto. Electron. Adv.* **2021**, *4*, 210017. [CrossRef]
136. Yankowitz, M.; Watanabe, K.; Taniguchi, T.; San-Jose, P.; LeRoy, B.J. Pressure-induced commensurate stacking of graphene on boron nitride. *Nat. Commun.* **2016**, *7*, 13168. [CrossRef]
137. Majumdar, A.; Dodson, C.M.; Fryett, T.K.; Zhan, A.; Buckley, S.; Gerace, D. Hybrid 2D Material Nanophotonics: A Scalable Platform for Low-Power Nonlinear and Quantum Optics. *ACS Photonics* **2015**, *2*, 1160–1166. [CrossRef]
138. Eda, G.; Maier, S.A. Two-Dimensional Crystals: Managing Light for Optoelectronics. *ACS Nano.* **2013**, *7*, 5660–5665.
139. Hao, R.; Jin, J.; Wei, X.; Jin, X.; Zhang, X.; Li, E. Recent developments in graphene-based optical modulators. *Front. Optoelectron.* **2014**, *7*, 277–292. [CrossRef]
140. Dushenko, S.; Ago, H.; Kawahara, K.; Tsuda, T.; Kuwabata, S.; Takenobu, T.; Shinjo, T.; Ando, Y.; Shiraishi, M. Gate-Tunable Spin-Charge Conversion and the Role of Spin-Orbit Interaction in Graphene. *Phys. Rev. Lett.* **2016**, *116*, 166102. [CrossRef]
141. Mendes, J.B.S.; Aparecido-Ferreira, A.; Holanda, J.; Azevedo, A.; Rezende, S.M. Efficient spin to charge current conversion in the 2D semiconductor MoS_2 by spin pumping from yttrium iron garnet. *Appl. Phys. Lett.* **2018**, *112*, 242407. [CrossRef]
142. Cao, Y.; Fatemi, V.; Demir, A.; Fang, S.; Tomarken, S.L.; Luo, J.Y.; Sanchez-Yamagishi, J.D.; Watanabe, K.; Taniguchi, T.; Kaxiras, E.; et al. Correlated insulator behaviour at half-filling in magic-angle graphene superlattices. *Nature* **2018**, *556*, 80–84. [CrossRef] [PubMed]
143. Cao, Y.; Fatemi, V.; Fang, S.; Watanabe, K.; Taniguchi, T.; Kaxiras, E.; Jarillo-Herrero, P. Unconventional superconductivity in magic-angle graphene superlattices. *Nature* **2018**, *556*, 43–50. [CrossRef] [PubMed]
144. Yankowitz, M.; Chen, S.; Polshyn, H.; Zhang, Y.; Watanable, K.; Taniguchi, T.; Graf, D.; Young, A.F.; Dean, C.R. Tuning superconductivity in twisted bilayer graphene. *Science* **2019**, *363*, 1059–1064. [CrossRef]
145. Cao, Y.; Rodan-Legrain, D.; Rubies-Bigorda, O.; Park, J.M.; Watanabe, K.; Taniguchi, T.; Jarillo-Herrero, P. Tunable correlated states and spin-polarized phases in twisted bilayer-bilayer graphene. *Nature* **2020**, *583*, 215–220. [CrossRef] [PubMed]
146. Zhang, S.; Song, A.; Chen, L.; Jiang, C.; Chen, C.; Gao, L.; Hou, Y.; Liu, L.; Ma, T.; Wang, H.; et al. Abnormal conductivity in low-angle twisted bilayer graphene. *Sci. Adv.* **2020**, *6*, eabc5555. [CrossRef]
147. Alexeev, E.M.; Ruiz-Tijerina, D.A.; Danovich, M.; Hamer, M.J.; Terry, D.J.; Nayak, P.K.; Ahn, S.; Pak, S.; Lee, J.; Sohn, J.I.; et al. Resonantly hybridized excitons in moire superlattices in van der Waals heterostructures. *Nature* **2019**, *567*, 81–86. [CrossRef]
148. Jin, C.; Regan, E.C.; Yan, A.; Iqbal Bakti Utama, M.; Wang, D.; Zhao, S.; Qin, Y.; Yang, S.; Zheng, Z.; Shi, S.; et al. Observation of moire excitons in WSe_2/WS_2 heterostructure superlattices. *Nature* **2019**, *567*, 76–80. [CrossRef]
149. Andrei, E.Y.; MacDonald, A.H. Graphene bilayers with a twist. *Nat. Mater.* **2020**, *19*, 1265–1275. [CrossRef]
150. Park, J.M.; Cao, Y.; Watanabe, K.; Taniguchi, T.; Jarillo-Herrero, P. Tunable strongly coupled superconductivity in magic-angle twisted trilayer graphene. *Nature* **2021**, *590*, 249–255. [CrossRef]
151. Park, J.M.; Cao, Y.; Watanabe, K.; Taniguchi, T.; Jarillo-Herrero, P. Flavour Hund's coupling, Chern gaps and charge diffusivity in moire graphene. *Nature* **2021**, *592*, 43–48. [CrossRef] [PubMed]
152. Li, X.; Zhang, S.; Wang, X.-J.; Huang, G.-F.; Xia, L.-X.; Hu, W.; Huang, W.-Q. A two-dimensional MoS_2/SnS heterostructure for promising photocatalytic performance: First-principles investigations. *Phys. E Low Dimens. Syst. Nanostructures* **2021**, *126*, 114453. [CrossRef]